CHAPTER 12: ANALYTICAL PROTOCOLS FOR ELEMENT CONCENTRATION AND ISOTOPE RATIO MEASUREMENTS IN FLUID INCLUSIONS BY LA–(MC–)ICP–MS

Thomas Pettke
University of Bern, Institute of Geological Sciences,
Baltzerstrasse 1+3,
CH–3012 Bern, Switzerland
E-mail: pettke@geo.unibe.ch

INTRODUCTION

Fluids are significant agents for transfer of chemical constituents and heat in the Earth. The only direct samples of ancient fluid flow are provided by fluid inclusions in minerals (*e.g.*, Roedder 1984). Successively entrapped fluid generations monitor evolution and are thus unique windows on fluid-assisted geological processes of the past.

The term fluid encompasses all phases that are not solid at the P–T–X (composition) conditions of the process of interest, including aqueous or carbonic solutions, silicate or sulfide or carbonate melts to name only a few geologically relevant ones. At earth surface conditions, we observe a vast diversity of physically and chemically distinct fluid phases. It decreases conspicuously with increasing P and T when various systems reach their critical endpoints, *e.g.,* the basalt–water system at *ca.* 5–6 GPa and 1000–1050°C where aqueous fluid and silicate melt become indistinguishable because the miscibility gap disappears (Kessel *et al.* 2005). Common to all these fluid systems is the observation that element solubilities tend to increase with increasing P and T. The chemical compositions of fluids provide key information to constraining fluid-mediated chemical cycling in the Earth.

Laser ablation (LA–) ICP–MS has become the most versatile *in situ* analytical technique to determine the elemental composition of many materials, and is the method of choice for the analysis of heterogeneous phase mixtures such as fluid inclusions in minerals. Historically, crush-leach techniques were first explored to characterize the metal contents dissolved in fluid inclusions, more than 40 years ago (Czamanske *et al.* 1963). Methods refinement has subsequently allowed the determination of the bulk aqueous fluid element and isotopic compositions present in fluid inclusions (*e.g.,* Bottrell *et al.* 1988, Banks *et al.* 1991, Pettke & Diamond 1995). However, these data only provided the composition of the mixture of various fluid stages present in the sample. Obviously, better sampling resolution is required to resolve properly different fluid stages commonly trapped in a given sample in order to refine our understanding of fluid-mediated processes in the Earth.

The *in situ* analysis of solutes from individual fluid inclusions was originally explored using destructive methods, *e.g.*, laser ablation (Tsui & Holland 1979, Bennett & Grant 1980, Deloule & Eloy 1982) or secondary ion mass spectrometry (SIMS; Nambu & Sato 1981). These early investigations detected the presence of metal ions in individual fluid inclusions, importantly also of ore metals for samples from hydrothermal ore deposits. In efforts to control the analysis of an individual fluid inclusion better and to detect its solute contents better, the analytical approaches have been varied significantly, from non-destructive techniques such as proton-induced X-ray emission (PIXE; Horn & Traxel 1987) to laser ablation connected to various detection devices, such as optical emission spectroscopy (OES; *e.g.,* Ramsey *et al.* 1992, Wilkinson *et al.* 1994; laser-induced breakdown spectroscopy, LIBS, Boiron *et al.* 1991) or inductively coupled plasma mass spectrometry (ICP–MS; Shepherd & Chenery 1995). SIMS was also further explored but the severe matrix-dependence of SIMS analysis combined with very long analysis times (*i.e.*, very slow ablation rate), limited penetration depth into the sample and very expensive instrumentation impeded its broader methods development (*e.g.*, Diamond *et al.* 1991). Further methods developments towards the quantification of solute contents in fluid inclusions then demonstrated that laser ablation combined with quadrupole ICP–MS (ICP–QMS) is most promising, with low UV laser wavelengths (*e.g.,* 193 nm ArF Excimer laser systems) and energy-homogenized beam profiles being most suitable for the controlled ablation of individual quartz-hosted fluid inclusions (Günther *et al.* 1998). The work by Günther *et al.* (1998) has established the analytical

---

Mineralogical Association of Canada Short Course 40, Vancouver, B.C., p. 189–217.

protocol for fluid inclusions, resulting in the first fluid chemical characterization of a Sn-ore forming system (Audétat *et al.* 1998). This was followed by a series of other applications to magmatic–hydrothermal fluids (*e.g.,* Heinrich *et al.* 1999, Ulrich *et al.* 2002, Audétat & Pettke 2003, Rusk *et al.* 2004, Stoffel *et al.* 2004, Landtwing *et al.* 2005, Hanley *et al.* 2005a, Banks *et al.* 2007, Klemm *et al.* 2007, 2008), metamorphic ore fluids (*e.g.,* Klemm *et al.* 2004) or basinal fluid migration (*e.g.,* Lüders *et al.* 2005). Applications to fluid inclusions have become broader as the LA–ICP–MS technique has become more accepted, *e.g.,* the first applications to experimental determination of fluid metal solubility (for Au: Loucks & Mavrogenes 1999, Simon *et al.* 2005; for PGE: Hanley *et al.* 2005b; for Sn: Duc-Tin *et al.* 2007; or even for transition metals such as Fe: Simon *et al.* 2004), or the analysis of metamorphic high-P fluid inclusions both from nature (*e.g.,* Scambelluri *et al.* 2004) and from experiment (*e.g.,* Spandler *et al.* 2007). The fundamental principles of the LA–ICP–MS analytical approach of Günther *et al.* (1998) for fluid inclusions has since remained largely unchanged; however, methods refinements have continuously improved the techniques. Cross-check against synthetic fluid inclusions of known composition has demonstrated that accurate fluid element concentrations can be obtained by LA–ICP–MS (Heinrich *et al.* 2003, Allan *et al.* 2005).

Halter *et al.* (2002) have expanded the LA–ICP–MS technique towards the analysis of individual, heterogeneous inclusions in any host phase, where the analysis of quartz-hosted fluid inclusions represents a specialized application. These authors published the mathematical procedures for signal deconvolution into pure host and pure inclusion including rigorous uncertainty estimation in great detail. This most general approach to the problem of signal quantification for entire inclusions drilled out of their host mineral has then been documented to be accurate at useful analytical precision based on melt inclusions from volcanic and shallow plutonic rocks (Pettke *et al.* 2004, Halter *et al.* 2004). This novel approach does not render homogenization efforts of melt inclusions obsolete, however, since reversed crystallization sequences and the temperature and mode of disappearance of the bubble provides essential petrologic information (*e.g.*, Bodnar & Student 2006). An update on approaches and methods for the analysis of individual, polyphase, entire, unexposed melt inclusions by LA–ICP–MS has recently been presented by Pettke (2006), and Mason *et al.* (2008) reports on latest developments in the field of melt inclusion analysis.

LA–ICP–MS has a key advantage, in that it allows independent optimization of two fundamentally different processes, (i) sample ablation and (ii) ion production, analyte filtering and signal recording in an ICP–MS. This is an enormous advantage over most other *in situ* analytical techniques (*e.g.,* SIMS or LIBS) where ion production or light emission is directly related to sample ablation. This dual optimization potential opens up the possibility for considerably reducing matrix effects on analyte signals. An instrument optimization strategy particularly focused on matrix-"insensitive" LA–ICP–MS chemical analysis of geological materials has been discussed by Pettke (2006). Following such a strategy, the need for matrix-matched calibration, which is essential for SIMS analysis and strongly recommended for electron probe microanalysis (EPMA), can be relaxed for LA–ICP–MS. This is the fundamental and, to date, unique analytical characteristic allowing for the bulk chemical analysis of heterogeneous phase mixtures such as fluid or crystallized melt inclusions in minerals. It must be appreciated, however, that the extent to which matrix effects can be minimized also strongly depends on the LA–ICP–MS setup considered (see Sylvester, 2008, for a detailed assessment).

Data reported in the literature are the outcome of the highly complex interplay between sample characteristics, laser ablation of fluid inclusions, ion production and signal recording. Each LA–ICP–MS instrumental set-up has its characteristic set of specifications, and these differ considerably between different set-ups. To generalize conclusions for LA–ICP–MS analysis is therefore not only delicate but also potentially misleading. It is therefore mandatory that instrumental parameters and settings, data reduction schemes, as well as sample characteristics, be reported in great detail so that results can be reproduced in other laboratories possessing closely similar analytical equipment. The large amount of precise data that can be produced in a short time may often belie potential problems in accuracy. Only critical assessment of data quality by every analyst and, more importantly even, also by every data user will help advance our understanding of how routine analytical procedures by LA–ICP–MS should best be done, which in turn will greatly increase comparability of published data sets.

This contribution focuses on the handwork of performing meaningful fluid inclusion analyses, reports on recent methods developments and refinements and will document relevant details of the analytical strategies. Essential characteristics of the special sample type "fluid inclusions" are outlined first. Relevant instrumental parameters and settings are discussed in detail, in order to achieve matrix-"independence" of analyte calibration, to maximize analyte sensitivities and to reduce element sensitivities selectively as may be required for quantification of fluid inclusion element concentrations. The various types of spectral interferences particularly relevant to fluid inclusion analysis are characterized.

In a second section, I elaborate on how to select, analyze and quantify a series of individual fluid inclusions belonging to a compositionally uniform fluid inclusion assemblage. Selection criteria for fluid inclusions suitable for LA–ICP–MS analysis are reported. The preferred technique of fluid inclusion ablation is then developed. Strategies for the most representative recording of fast transient signals produced from polyphase fluid inclusions for single detector (*i.e.,* sequential data recording) mass spectrometers are evaluated. The data reduction scheme for obtaining element concentration data of fluid inclusions is then discussed step by step, and the data are evaluated with respect to precision and accuracy. Procedures to improve significantly on limits of detection (LOD) for individual fluid inclusion analysis are described.

In a third section, I report the analytical strategy for Pb isotopic ratios of individual fluid inclusions using LA–MC–ICP–MS and address the figures of merit currently obtained. The chapter then concludes with a detailed assessment of the statistical relevance of concentration and isotope ratio data sets obtained for fluid inclusions.

The new procedures for elemental and isotopic analysis of individual fluid inclusions reported herein shall aid in achieving accurate data at useful external reproducibility. For fluid inclusion assemblages, average solute concentrations with ±5% 1 SD (standard deviation) uncertainties can be achieved. Uncertainties on inclusion to inclusion reproducibility of a natural fluid inclusion assemblage (n=11) approached 0.07% 2 SD for ^{208}Pb/^{206}Pb and ^{207}Pb/^{206}Pb ratios and 0.14% 2 SD for Pb isotope ratios normalized to mass 204, respectively, and these isotope ratio data are accurate.

FLUID INCLUSIONS: CHARACTERISTICS RELEVANT FOR THEIR LA–ICP–MS ANALYSIS

Fluid inclusions are commonly trapped as a single phase at elevated temperatures and pressures (exceptions are heterogeneous entrapment in a two or more phase stability volume; *e.g.,* Roedder 1984). Key to the usefulness of fluid inclusions (and melt inclusions) is that after entrapment, the inclusions behaved as a chemically closed system, *i.e.,* individual fluid inclusions do not lose or gain chemical components[1].

Figure 12-1a shows a typical fluid inclusion assemblage. As can be seen, an individual fluid inclusion consists of several phases. After formation, daughter minerals crystallize and other phases (*e.g.,* a vapor bubble) unmix from the initially homogeneous phase while the fluid inclusion cools to room temperature. It is this polyphase sample of confined volume that we wish to analyze altogether in order to reconstitute the bulk chemical composition of the fluid inclusion at the time of entrapment. It is therefore crucial not to lose any fraction of the fluid inclusion content (solids or liquids or gases) and to analyze all the different phases present within an inclusion quantitatively. Partial ablation of a fluid inclusion will inevitably provide measurements that return data of which only a few element concentrations may be deemed correct, at best.

Fluid or melt inclusion assemblages (Goldstein & Reynolds 1994), per definition, are a series of fluid inclusions entrapped at the same time in a host mineral. Petrographically, geometric features are employed to argue for coeval entrapment of fluid inclusions, *e.g.*, the entrapment of fluid inclusions along a host mineral growth zone or a fracture plane. We distinguish homogeneous entrapment and heterogeneous entrapment. Homogeneous entrapment implies that a compositionally uniform single phase fluid was entrapped. Heterogeneous entrapment implies that two coexisting fluid types (*i.e.*, chemically distinct fluids) were coevally entrapped, forming, for example, a boiling assemblage where liquid and vapor inclusions coexist. Throughout this chapter, I refer to homogeneously entrapped fluid inclusion

---

[1] Discussion of the real case where post-entrapment modification of fluid inclusion contents may have occurred (e.g., Sterner & Bodnar 1989, Audétat & Günther 1999, Bodnar 2003, Klemm et al. 2007) is beyond the scope of this paper.

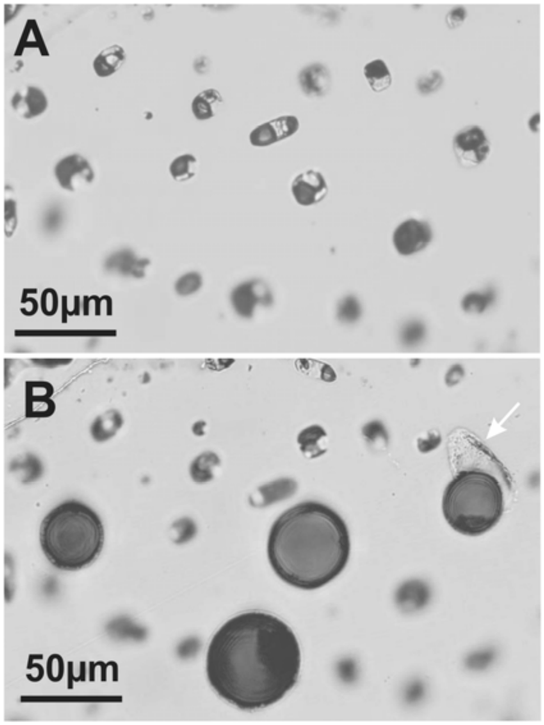

FIG. 12-1. **a)** Brine fluid inclusion assemblage in quartz from a stockwork vein of a porphyry-Cu deposit, Rosia Poieni, Romania (focused below sample surface). Note the uniform phase proportions between individual inclusions, petrographically indicating that they are compositionally identical. **b)** Sample after analysis of 4 inclusions from this assemblage (focused on sample surface), demonstrating the highly controlled laser ablation of individual fluid inclusions with the GeoLas system used. This is the ideal case.

assemblages unless stated explicitly otherwise.

Let us take the fracture as an example of how inclusions formed. The fracture was filled with a one-phase fluid and then started to heal, thereby forming a series of individual fluid inclusions, each trapping a fraction of the homogeneous fluid that filled the fracture. Ideally, individual fluid inclusions have been isolated (*i.e.*, sealed) while the fluid was still in the one phase field. Each individual fluid inclusion therefore represents an isolated sample of this homogeneous fluid, and all individual fluid inclusions of an assemblage are thus compositionally identical. Evidence of this can be seen petrographically by identical phase proportions at room temperature (illustrated in Fig. 12-1a), and it can be corroborated by consistent microthermometric results. The analysis of a series of fluid inclusions belonging to a fluid inclusion assemblage therefore allows for repetitive analysis of a compositionally uniform sample (identical to analyzing several spots on a homogeneous solid). Consequently, the fluid composition is best characterized as the average plus external uncertainty of the individually analyzed fluid inclusions from the homogeneously entrapped assemblage. This provides the most robust characterization of element compositions in the fluid at the time of entrapment, *i.e.,* at a given stage of fluid evolution in the system of interest. The main analytical challenge is therefore to determine the composition of a homogeneous fluid phase based on the analysis of a series of micro-samples of a confined, heterogeneous phase mixture of *a priori* unknown mass proportions.

Note that even apparently simple aqueous or aqueo-carbonic (Fig. 12-2a) or vapor fluid inclusions (Fig. 12-2b) may contain a major proportion of some trace elements concentrated in a tiny daughter mineral that may be too small for microscopic detection or simply hidden by the large vapor bubble. It is therefore mandatory that the entire fluid inclusion is ablated in a controlled manner and analyzed completely.

SPECIFIC LA–ICP–MS INSTRUMENTAL REQUIREMENTS FOR FLUID INCLUSION ANALYSIS

Before turning to relevant aspects of the handwork of fluid inclusion analysis by LA–ICP–MS, the analytical setup used for obtaining most of the data shown here will be characterized first. This is essential as each analytical setup has its advantages and drawbacks; hence, the problems to be solved determine which setup will most likely provide the overall best analytical performance. The system at the University of Bern consists of a GeoLas Pro 2006 (Lambda Physik, Germany) pulsed 193 nm ArF excimer laser system coupled with an ELAN DRC-e ICP quadrupole mass spectrometer (Perkin Elmer, Canada). Typical settings for fluid inclusion analysis using this setup are reported in Table 12-1. The GeoLas Pro system is operated exclusively in manual mode. Energy densities on the sample surface are homogeneous irrespective of ablation crater size, adjustable to between 4 and 200 µm. Crater sizes below 8 µm and above 120 µm are generally not relevant for fluid inclusion analysis, since complete ablation of the entire fluid inclusion is a prerequisite for obtaining relevant compositional data, and inclusions larger than *ca.* 50 µm do not return improved LODs (see below).

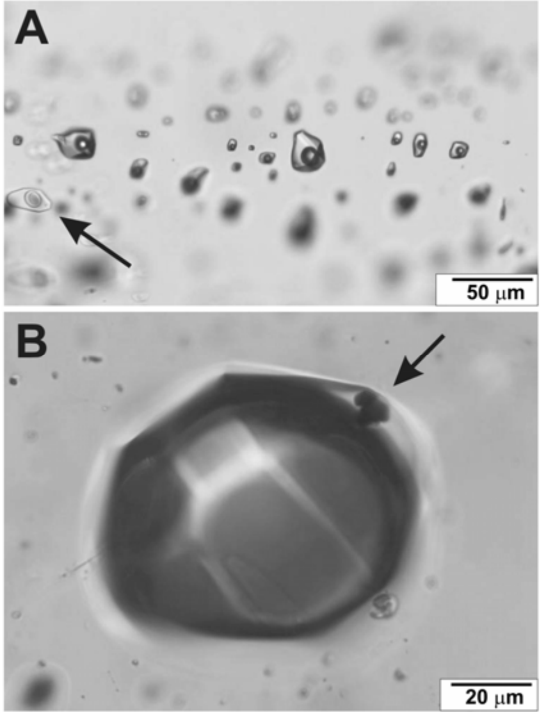

FIG. 12-2. **a)** Assemblage of three-phase CO_2-rich inclusions from auriferous quartz veins, Brusson, NW Italy (Diamond 1990, Pettke *et al.* 2000a). Note the flat inclusion (black arrow) that shows menisci of $CO_{2,\ liquid}$ and $CO_{2,\ vapor}$ in aqueous solution. **b)** Large vapor inclusion with a thin rim of aqueous liquid wetting the inclusion walls and containing opaque daughter crystals (black arrow, in focus). It is obvious that such tiny daughter crystals can escape petrographic recognition when they are beneath the vapor bubble or out of focus during petrographic inspection.

The principle for fluid inclusion analysis by LA–ICP–MS is simple. A polished sample thick section is placed in an ablation cell, together with an external standard material. A laser beam is used to completely drill out individual fluid inclusions; the liberated material forms an aerosol that is carried by the aerosol carrier gas into the ICP where ions are produced. Cations are then analyzed according to their mass to charge (m/z) ratios on a detection device. Measurement data are read out as transient (*i.e.,* time resolved) signal intensities, preferably in counts or volts, depending on the type of detector used. These machine data are then converted off-line into element ratio, element concentration or isotope ratio data employing various data reduction protocols.

In summary, accurate LA–ICP–MS measurements of geological materials including multiphase inclusions should obviously follow the

TABLE 12-1: LA–ICP–MS INSTRUMENT AND DATA ACQUISITION PARAMETERS

GeoLasPro 193 nm ArF excimer laser (Compex 102 Pro)	
Laser fluence on sample	24 J/cm^2, homogeneous energy distribution
Pulse duration	15 ns
Repetition rate	10 Hz
Pit sizes	Between 8 and 90 µm
Ablation cell volume	7 cm^3
Ablation cell gas flows	1.0 L min^{-1} He, 0.008 L mi n^{-1} H$_2$

ELAN DRC-e quadrupole ICP–MS	
Nebulizer gas flow	0.83 L min^{-1} Ar
Auxiliary gas flow	0.70 L min^{-1} Ar
Cool gas flow	16.0 L min^{-1} Ar
rf power	1450 kV
rPa value	0
rPq value	0.25
Detector mode	Dual (cross-calibrated pulse / analog modes)
Quadrupole settling time	3 ms
Detector housing vacuum	4.5 – 6.5 *10^{-6} Torr during analysis
Oxide production rate	Tuned to <0.5% ThO
Robust plasma conditions	Tuned to S(U) = S(Th)

Data acquisition parameters	
Sweeps per reading	1
Readings per replicate	600
Replicates	1
Dwell time per isotope	10 ms, except for ^{29}Si = 8 ms
Points per peak	1 per measurement
Isotope sequence analyzed in jump routine	^{23}Na, ^{197}Au, ^{29}Si, ^{197}Au, ^{35}Cl, ^{197}Au, ^{39}K, ^{197}Au, ^{55}Mn, ^{197}Au, ^{57}Fe, ^{197}Au, ^{65C}u, ^{197}Au, ^{88}Sr, ^{197}Au, ^{95}Mo, ^{197}Au, ^{207}Pb, ^{197}Au

Note: S stands for sensitivity

philosophy of keeping all parameters as uniform as possible in order to minimize the potential for complications. A series of relevant parameters to be considered was provided by Pettke (2006) and are briefly summarized as follows:

- Best possible visualization of sample on TV screen during laser ablation sampling
- Sufficient laser energy density on sample at appropriate wavelength to controllably ablate all matrices of interest
- Homogenized energy density across tunable ablation crater sizes, to minimize ablation energy dependent changes in aerosol production and to maximize control of the ablation process notably for bulk inclusion analysis.
- Robust plasma conditions, to maximize matrix independence of analytical conditions (external calibration)
- Maximize analytical signal to noise ratios, and not only sensitivity
- Constant and low backgrounds to minimize LOD
- Representative recording of short transient signals as commonly produced from ablation of inclusions
- Proper analyte selection for minimizing polyatomic interference problems

Step 1: Laser ablation of fluid inclusions

For liberation of the fluid inclusion content, a monochromatic, collimated, coherent, pulsed laser beam is used. Wavelengths in the low UV are preferred nowadays, because the absorption of light generally increases with decreasing wavelength for silicate and oxide phases commonly hosting fluid inclusions. Laser beams in Q-switched mode (*i.e.,* pulsed) are preferred, as they allow for establishing the desired ablation rate at constant energy density on the sample surface, they reduce (nanosecond lasers) or eliminate (femtosecond lasers) negative interactions between aerosol expanding above the ablation spot and incoming laser light, and sample heating around the ablation spot is minimized. Laser systems delivering a homogeneous energy distribution across the entire ablation spot are strongly preferred, because they allow for choosing the appropriate beam size for fluid inclusion ablation at constant energy density (thus eliminating any energy–density-related fractionation at the ablation site). They also enhance the control of the fluid inclusion ablation process by minimizing cracking of the host mineral and associated catastrophic liberation of the fluid inclusion contents during ablation.

Laser ablation of fluid inclusions, as for other samples, is also best done in a He atmosphere because sample deposition around the craters is greatly reduced when using He instead of Ar as ablation chamber gas (Eggins *et al.* 1998, Günther & Heinrich 1999). This in turn maximizes the fraction of ablated material that can be transported to the ICP.

Aerosol transport system

The aerosol transport system encompasses the ablation chamber (or ablation cell) and the transport tubing to the injector tube. The ablation chamber must accommodate the sample and reference material(s) and should be characterized by minimal washout times. The latter translates into higher signal to background intensity ratios for the transient signal interval of a given fluid inclusion ablation, resulting in improved LODs. Interestingly, the length of the tubing connecting the ablation chamber to the torch has a subordinate influence on the overall shape of the transient signal (Venable & Holcombe 2001) – signal dispersion is almost exclusively dominated by gas flow conditions inside the ablation chamber (*e.g.*, Günther 2001). For fluid inclusions, we commonly use either a 1 cm^3 or a *ca.* 7 cm^3 ablation chamber with optimized washout times (documented in Fig. 12-3).

Prior to the ICP torch, the "Nebulizer Ar gas stream" needs to be admixed to the aerosol-in-He gas stream, because mixed He–Ar aerosol carrier gas is required to maintain a stable plasma. The connector used to admix the Ar delivered by the "Nebulizer gas flow" consists in our case of a simple y-piece where the aerosol-bearing He is blown into the Ar flow using a syringe needle, and the mixture then flows into the torch (Fig. 12-4). This setup ensures perfect mixture between Ar and the aerosol-bearing He but has the disadvantage that it is prone to particle accumulation, particles that may then cause signal spikes in subsequent analyses that must be eliminated for quantification (more below).

Step 2: Ion production and recording

In principle, all the sample material reaching the ICP should be completely converted to singly charged cations, and all these cations should be recorded on the detection device. Obviously, reality is very far from this ideal. It is therefore the challenge for the analyst to optimize the ICP–MS

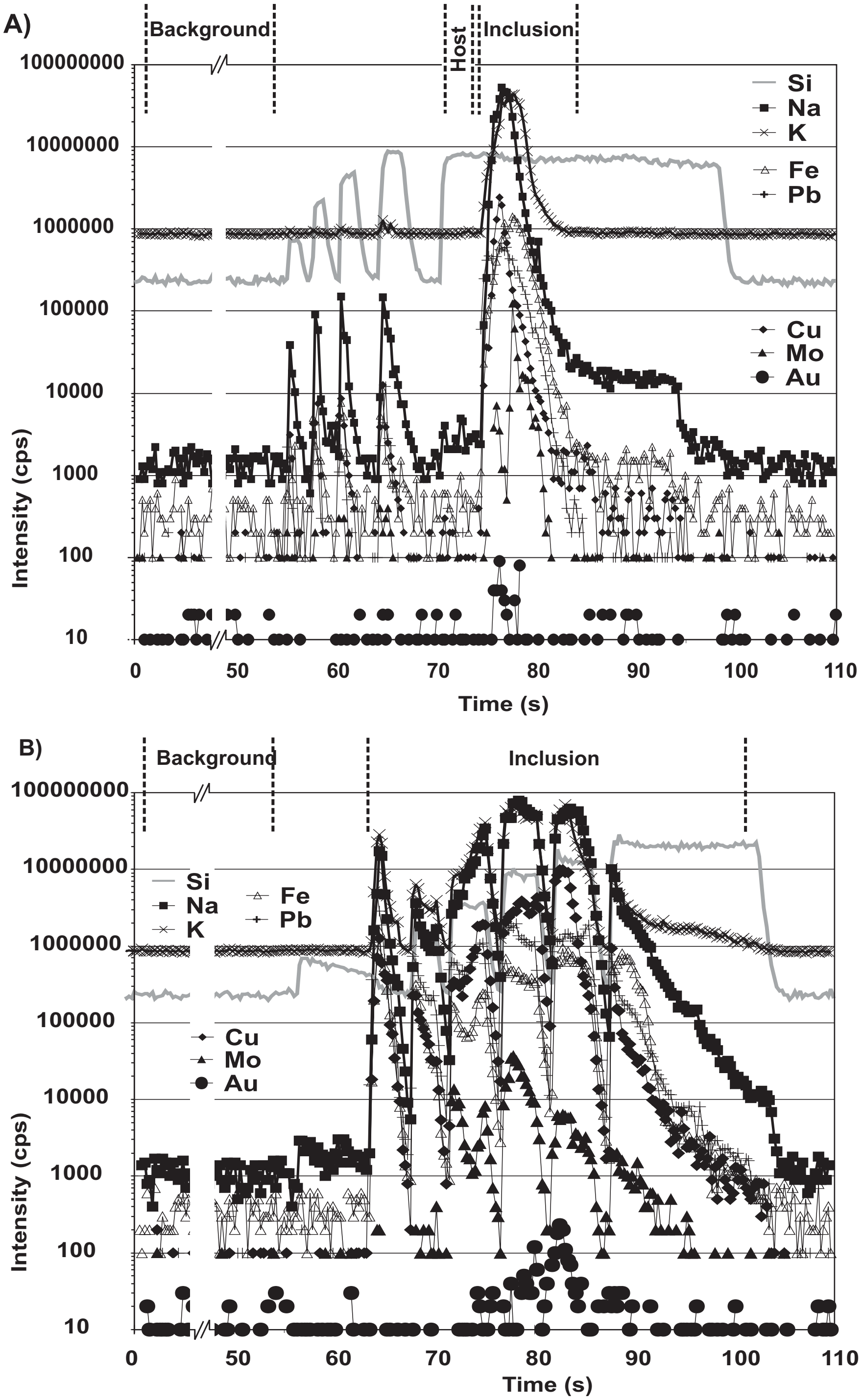

FIG. 12-3. Transient LA–ICP–MS signals of individual fluid inclusions, with signal count rates shown in logarithmic scale. Background, Host and Inclusion refer to the respective signal intervals used for quantification. **a)** Signal of a polyphase brine inclusion resulting from the straight ablation method (inclusion 14fre11, Table 12-3). Note the surface contamination (these are deposits from previous fluid inclusion ablations nearby in this case) at every crater size increase. **b)** Signal of a polyphase brine inclusion produced by the stepwise fluid inclusion opening procedure (inclusion from Bingham Cu–Au±Mo porphyry vein). For this inclusion, a host quartz signal needs to be measured separately nearby. (Continued on next page.)

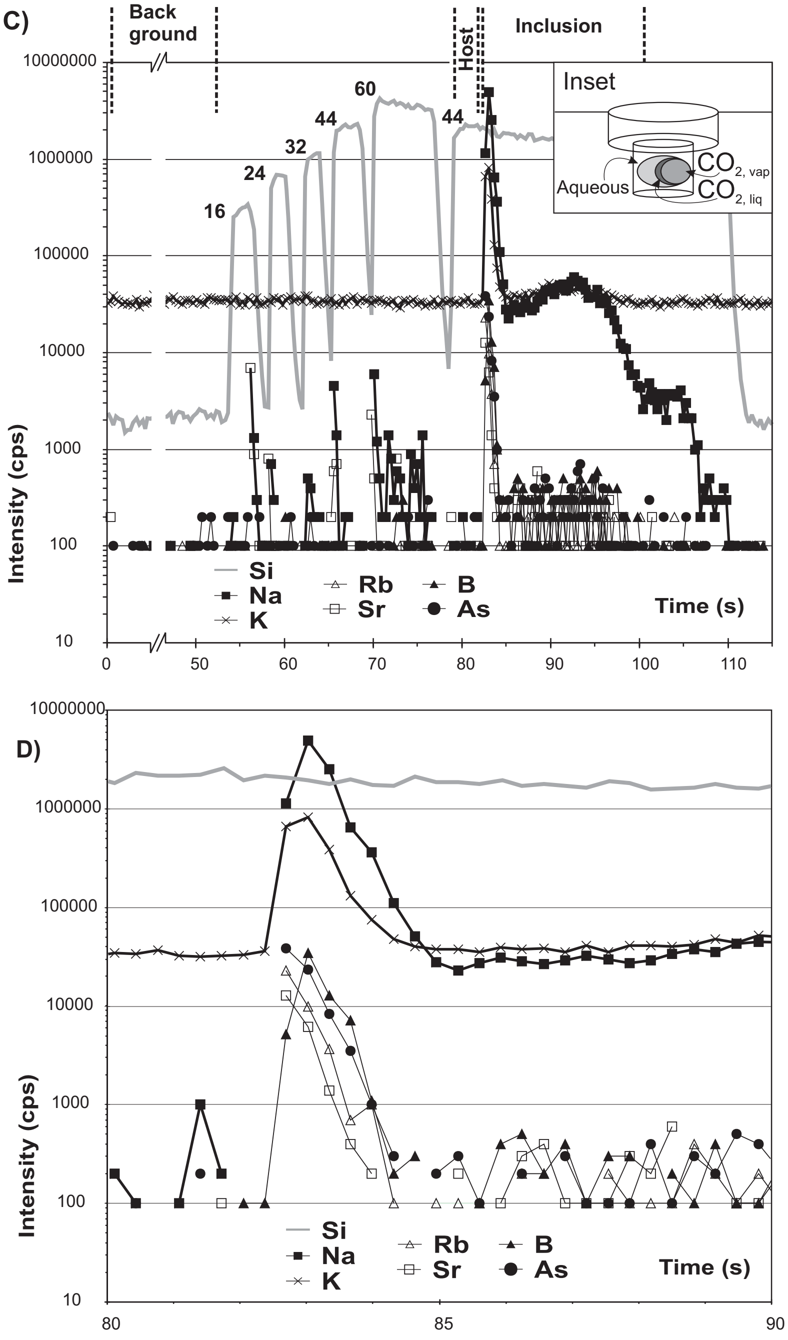

FIG. 12-3 (contd.). Transient LA–ICP–MS signals of individual fluid inclusions, with signal count rates shown in logarithmic scale. Background, Host and Inclusion refer to the respective signal intervals used for quantification. **c)** Characteristic swan-shaped signal for the analysis of a three-phase CO_2-rich fluid inclusion released by straight ablation, after having step-wise increased the pit size (labeled next to the grey Si signal) to a larger diameter than that finally used for fluid inclusion ablation (see inset). This technique can be employed to remove host material lying above deeper inclusions in order to minimizing negative side effects encountered for craters with a high depth to diameter ratio (exceeding *ca.* 2), such as signal tailing. Note the extremely fast transient signal maximum at fluid inclusion opening (see enlargement of signal shown in **d)** that probably results from increased internal pressure in response to heating induced by laser light reaching the inclusion before opening. This analysis has been acquired without H_2-mode. Also note for figures **a)** to **c)** the fast signal decay after the laser was switched off, documenting a washout time of about 3 s.

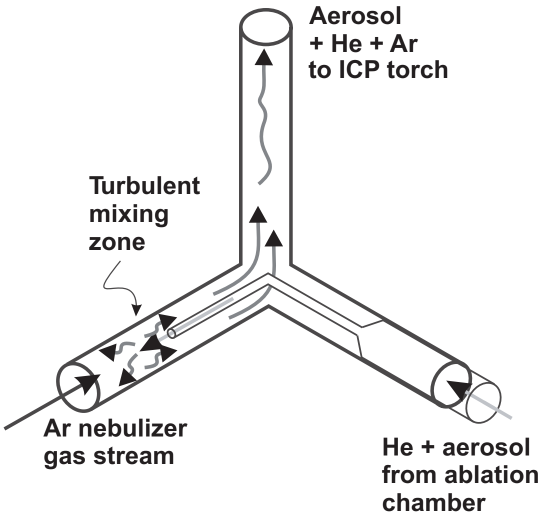

FIG. 12-4. Drawing of the Y piece used to mix the aerosol_in-He stream with the nebulizer Ar gas stream prior to entering the torch.

instrumental part such that the cations recorded on the detector are representative for the sample analyzed. This sounds simple, but it is far from trivial.

<u>Optimization of the ICP–MS parameters:</u> The simple function of the ICP is to convert the aerosol particles to atoms and to ionize these. In practice, most recent research has demonstrated that this is currently the instrumental weak point in LA–ICP–MS analysis in general (*e.g.,* Günther & Hattendorf 2005). Most well known in LA–ICP–MS are problems collectively referred to as elemental fractionation, *i.e.*, changes of element responses (*i.e.,* element sensitivity ratios) with changing LA–ICP–MS analytical conditions (*e.g.,* Longerich *et al.* 1996a), and, for isotopic ratio analysis, mass bias. Elemental fractionation historically has been assigned to processes occurring at the laser ablation site (*e.g.,* Fryer *et al.* 1995, Mank & Mason 1999), and only recently has it become apparent that plasma processes are equally – if not dominantly – responsible for elemental fractionation (*e.g.,* Guillong & Günther 2002).

This insight has encouraged Günther & Hattendorf (2005) to establish optimization criteria for "**robust plasma conditions**"; simply speaking, conditions where ion production in the ICP is uniform and as complete as possible. At such ICP conditions, fractionation effects resulting from incomplete ionization are minimized. Pettke (2006) has summarized the aspects relevant for the analysis of polyphase inclusions in detail and introduced this approach as a means of minimizing matrix-dependency of external calibration. Briefly, the ICP–MS is optimized daily for maximum signal to noise ratios (and not only sensitivity) across the entire mass range of interest, at low element oxide production levels commonly monitored using the ThO production rate. These settings are then tested for equal sensitivity of Th and U, two elements with nearly equal first ionization energies, mass, and abundance of major isotopes. The SRM 610 and 612 glasses from NIST are ideal for this as they possess largely equal U and Th concentrations; thus, the ^{238}U/^{232}Th intensity ratio should be one. Günther & Hattendorf (2005) demonstrated that ICP–MS optimizations based on maximum sensitivity and ThO/Th < 0.5% may return U/Th sensitivity ratios much higher than one, indicative of non-uniform aerosol ionization. Analyzing samples with such an ICP–MS setting would therefore require matrix- and crater size-matched external standardization, conditions at which such fractionation processes would be closely comparable between sample and external standard and thus cancel. A matched external calibration approach grossly limits the versatility of LA–ICP–MS analysis, however, and it is not practical for the analysis of polyphase fluid inclusions in complex silicate host minerals. Capillaries containing aqueous solutions compositionally similar to the inclusions to be analyzed have been proposed as an improved external calibration strategy (*e.g.,* Stoffel *et al.* 2004). While the standard matrix more closely approaches the sample when compared to the use of SRM 61X glasses, there are caveats regarding some aspects of this approach. Experiments in our lab have revealed that element sensitivity ratios obtained from the ablation of solutions in capillaries may vary as a function of the focusing depth of the laser beam (*i.e.*, the z-axis). Capillaries are commonly thicker than *ca.* 50 µm; hence, using a crater size similar to that employed for fluid inclusion ablation returns a crater aspect ratio (depth to diameter ratio) that exceeds one, conditions at which fractionation at the laser ablation site may become relevant. The content of capillaries is also not sampled completely for calibration (capillaries are simply too large in volume), thus not allowing for complete sampling of the solution as required for fluid inclusion analysis (more below). Finally, the bulk mass analyzed during complete inclusion ablation corresponds to largely equal proportions of matrix mineral and inclusion content (*e.g.,* Halter *et al.*

2002, Pettke 2006); hence, the analyzed aerosol represents a mixture of silicate, water and salts for which external calibration based on SRM 61X glasses returns accurate fluid inclusion data (*e.g.,* Heinrich *et al.* 2003).

That matrix-independent external calibration can be achieved through careful ICP optimization has been demonstrated in the literature, *e.g.,* for silicate minerals by Jackson *et al.* (1992), for aqueous fluid inclusions (Günther *et al.* 1998, Heinrich *et al.* 2003), oxides (*e.g.,* Heinrich *et al.* 2003), carbonates (*e.g.,* Eggins *et al.* 2003) and even for Fe, Ni, Co and Cu in some sulfides (chalcopyrite, pyrrhotite and millerite; Halter *et al.* 2004). Having fit for purpose instrumentation and following ICP–MS optimization criteria to establish robust plasma conditions (Günther & Hattendorf 2005) for minimizing matrix dependence will provide the versatility needed for the analysis of polyphase inclusions in minerals (Pettke 2006).

Analyte sensitivities: It has long been recognized that sensitivity in dry aerosol mode LA–ICP–MS (50 µm crater size) is about three orders of magnitude lower than what can be achieved in solution mode ICP–MS (*e.g.*, Günther *et al.* 1997). Consequently, LODs are also significantly higher than in solution mode, despite overall much lower gas background intensities. Sensitivity enhancement is therefore central to improving the detection capability in LA–ICP–MS. Commonly such sensitivity enhancement can be achieved for LA–ICP–MS with a few modifications such as the use of He in the ablation chamber (*e.g.,* Eggins *et al.* 1998) or the reduction of the interface pressure (Günther *et al.* 1997). Recently, Guillong & Heinrich (2007a) demonstrated an up to 7-fold, element-specific increase in sensitivity through the addition of small amounts of H_2 to the aerosol carrier gas on their GeoLas 193 nm LA–ICP–MS system (Elan 6100 DRC). Not only the analyte signals but also the gas backgrounds are variably affected by the above modifications. The sum of these effects will determine whether an improvement in signal to noise ratio can be achieved on a given LA–ICP–MS instrumental setup, potentially significantly lowering the LODs and improving the external reproducibility of ultra-trace element measurements. Implementing H_2 addition to the aerosol carrier gas following Guillong & Heinrich (2007a), sensitivities achieved on our Elan DRCe QMS are reported in Table 12-2. Since gas backgrounds deteriorate for only a subset of m/z commonly used for analysis, an improvement in LOD results also for most elements commonly analyzed in fluid inclusions.

TABLE 12-2: ELEMENT SENSITIVITIES

	Mass analyzed	Sensitivity (cps per µg g^{-1})
Na	23	1400
Si	29	520
K	39	2400
Mn	55	3300
Fe	57	3600
Cu	65	2700
Sr	88	4800
Mo	95	4000
Pb	208	6700
Au	197	3400

Analytical conditions as in Table 12-1
Pit size = 44 µm
Reference material: SRM 612

For fluid inclusion analysis, we aim at analyzing for major to trace elements (*i.e.,* from tens of wt.% to ng g^{-1} concentrations). In order to cope with such an extreme range in signal intensities, even cross-calibrated dual detector systems providing up to 9 orders of magnitude linear dynamic range may become insufficient for some applications. Among the major elements in fluid inclusions, Na is often the major constituent (recall that the bulk salinity of fluid inclusions is commonly expressed as wt.% equivalent NaCl). Element-specific mass resolution (as can be calibrated in an Elan ICP–QMS) can selectively lower the sensitivity on a given isotope (*e.g.*, Heinrich *et al.* 2003). These authors presented the analysis of 1 ng g^{-1} U in halite as an example, a situation where a linear dynamic range of the detector exceeding 9 orders of magnitude would have been required to solve this analytical challenge. This becomes more of a concern notably because sensitivities in laser ablation mode are getting better and because major elements are commonly used as the internal standard elements for signal quantification (more below).

The range in signal count rates required to analyze an individual inclusion for major (up to several tens of wt.%; Table 12-3), minor and trace elements (down to tens of ng g^{-1} possible in the best case) can also be reduced by using element-specific bandpass filtering as available in dynamic reaction cell (DRC) technology implemented in some Elan ICP–QMS instruments (see Tanner & Baranov 1999, for the theory of operation). This approach is

TABLE 12-3: ELEMENT CONCENTRATION DATA OF INDIVIDUAL FLUID INCLUSIONS OF ONE FLUID INCLUSION ASSEMBLAGE FROM A PORPHYRY STAGE QUARTZ VEIN OF GRANISLE

Shot number	**Ablation quality**	**Ablation mode SW; straight**	**Au signal visible Y=yes; N=no†**	**FI size µm**	**Na µg/g**	**K µg/g**	**Mn µg/g**	**Fe µg/g**	**Cu µg/g**	**Sr µg/g**	**Mo µg/g**	**Pb µg/g**	**Au µg/g**
14frc03	++(+)	STRAIGHT	N	26	107300	116200	13400	133300	9100	290	390	1870	<0.028
14frc04	+++	STRAIGHT	Y	22	117400	110800	12600	115900	*12100*	240	340	1680	0.069
14frc06	+++	STRAIGHT	Y	25	110500	121400	12700	122400	6800	230	300	1680	0.054
14frc07	++(+)	STRAIGHT	Y	25	129100	99400	10700	101000	6600	210	310	1510	0.024
14frc08	+++	STRAIGHT	N	18	112300	117300	13900	120600	5600	280	380	1850	<0.072
14frc09	+++	STRAIGHT	N	25	136300	82900	10000	99600	5000	200	210	1290	<0.066
14fre10	+++	SW	Y	25	128000	99700	11200	102900	7400	240	280	1370	*0.087*
14fre11	+++	STRAIGHT	Y	20	112200	116100	12600	123200	7800	260	350	1520	0.064
14fre12	+++	STRAIGHT	Y	32	121300	109800	11700	109000	*18500*	210	310	1500	0.053
14fre13	+++	STRAIGHT	Y	25	116500	110400	12200	118700	3400	250	310	1500	*0.100*
14fre14	+++	SW	Y	25	128800	99700	10100	102200	3600	210	250	1280	0.026
15frb03	+++	SW	Y	20	114700	124300	12000	111200	7800	250	290	1380	0.041
15frb04	+++	STRAIGHT	Y	20	112100	128400	11900	113600	*20000*	260	330	1530	0.039
15frb05	++(+)	STRAIGHT	Y	28	127900	108700	10200	96300	6400	220	260	1320	0.054
15frb06	+++	STRAIGHT	Y	15	101200	143300	13600	124000	6500	290	230	1770	0.068
15frb07	+++	STRAIGHT	Y	25	112500	128300	11900	112800	*21400*	240	350	1450	0.056
15frb08	+++	SW	Y	35	125300	117000	10500	95000	3900	190	260	1250	0.040
15frb09	+++	STRAIGHT	N	18	130500	108800	10200	90600	4200	220	270	1340	<0.058
15frb10	+++	STRAIGHT	N	15	103900	134200	14300	125000	5900	270	230	1800	<0.089
14frc05	++	*STRAIGHT*	*Y*	*24*	*59300*	*198900*	*19700*	*165400*	*16500*	*270*	*370*	*2210*	*0.052*
				average	118305	114600	11900	111400	6000	240	300	1520	0.049
				1 stdev	9966	14000	1300	12000	1700	30	50	200	0.015
				1 sterr	2286	3212	298	2753	439	7	11	46	0.004
				1 stdev %	8%	12%	11%	11%	28%	13%	17%	13%	31%
				1 sterr %	1.9%	2.8%	2.5%	2.5%	7.3%	2.9%	3.8%	3.0%	8.8%

Sample used is GI-13-17. Equivalent NaCl concentration used as the internal standard for signal quantification is 55 wt.%. Isotopes analyzed are listed in Table 12.1

Values *in italic* are deemed outliers and thus have not been used for statistical calculations (as explained in text)

+++	indicates perfect ablation of fluid inclusion
++(+)	indicates good ablation of fluid inclusion with a very minor problem (e.g., signal tailing because the fluid inclusion was deep)
++	indicates acceptable ablation, with problems such as surficial quartz breakout or unclear signal boundary because an underlying inclusion was hit before the first signal ended
STRAIGHT	indicates straight ablation (see Fig. 3a, c and text for explanations)
SW	indicates stepwise opening (see Fig. 3b and text for explanations)
†	indicates whether a gold signal is visible in the transient signal plot (Y) or not (N)
<value I	indicates that the concentration value is below the LOD, calculated using the 3 σ criterion (Longerich et al., 1996) as explained in text

more versatile as it does not require a separate calibration of an element-specific resolution. All that is required is to optimize the RPa and RPq values to achieve the desired element-specific reduction in sensitivity, *i.e.,* bandpass filtering. The analysis of the external calibration and sample material at these conditions will then allow for the use of the major element as the internal standard, such as Na for trace elements in halite (see Heinrich *et al.* 2003). Another approach to avoid problems created from too intense analyte signals could be to optimize the ion extraction lenses such that the sensitivities of low m/z elements (*i.e.,* the common major elements) are suppressed – however, this suppresses the sensitivities of low m/z trace elements alike; hence, it is not considered to be a method of choice.

Spectral interferences also plague LA–ICP–MS analysis. However, they are less of a problem than in many other spectrometric detection devices. Since we always have *all the matrix all the time* during analysis, matrix-related interferences are most problematic, and their effects are possibly often underestimated.

Isobaric interferences are considered to be "easy" types of interferences. Sometimes, they can easily be avoided by proper isotope selection (and often accepting significantly elevated LODs, *e.g.,* for Ca). If not feasible, isobaric overlap can be corrected for mathematically provided that the interfering cation is part of a stable isotope pair (*e.g.,* ^{106}Cd on ^{106}Pd as derived from in-run measured ^{110}Cd). For cases where the interferent is far subordinate in intensity, a simple subtraction of interferent count rate may be tolerable. For cases where the interferent signal is a considerable fraction of the total signal, notably in the low mass range or for highly accurate isotope ratio measurements, the mathematical interference subtraction must be based on a mass-bias corrected interferent isotope ratio (see below).

Gas interferences from plasma gas and entrained air (*e.g.,* adsorbed on ablation chamber and aerosol transport system or entrained into the atmospheric pressure ICP) are accounted for by background subtraction (*e.g.,* ^{12}C^{16}O^{1}H or ^{13}C^{16}O or ^{14}N^{15}N on ^{29}Si). Finally, care has to be taken to avoid doubly charged ions (recall that the mass filter of an ICP–MS resolves ions according to their mass/charge ratio), notably since second ionization potentials of some elements are lower than the first ionization potentials of other elements, *e.g.,* doubly charged light rare earth elements (LREE) producing interferences on Ga, Ge, As or Se. For LREE-enriched fluid, as can be expected for some pegmatites or for LREE-rich accessory minerals, interferences of ^{150}Nd^{2+} (10.73 eV 2nd ionization potential) and ^{150}Sm^{2+} (11.07 eV 2nd ionization potential) may render the analysis of ^{75}As (9.79 eV 1st ionization potential) problematic. Similarly, trace ^{45}Sc in zircon cannot be analyzed using low resolution mass spectrometry because of the ^{90}Zr^{2+} overlap. Using the H_2 admixture to the aerosol carrier gas described above also results in an increased M^{2+} production rate (*e.g.,* Ca^{2+} from 0.6% to *ca.* 1.2% on our system; similar to that reported by Guillong & Heinrich 2007a). This should be taken into consideration for analyte selection especially when using the H_2 mode.

Problematic interferences are polyatomic ions that form by combination of elements abundant in the plasma gas with elements abundant in the analyzed matrix. Element oxides also belong to this group simply because oxygen is the most abundant element in silicates. Metal argides ((M^{40}Ar)$^{+}$) are always a concern, *e.g.,* ^{55}Mn^{40}Ar on ^{95}Mo for magmatic–hydrothermal fluids where Mn is a major cation, or ^{65}Cu^{40}Ar on ^{105}Pd for magmatic–hydrothermal fluids or Cu-rich sulfides, or ^{12}C^{12}C, ^{12}C^{13}C, ^{13}C^{13}C on ^{24,25,26}Mg in aqueo-carbonic fluids or carbonates. Importantly, these types of interferences are not only produced from sample– gas interaction but equally so from standard–gas interaction, *e.g.,* ^{63}Cu should not be calibrated using the SRM 612 glass because of the ^{23}Na^{40}Ar polyatomic interference resulting from the >13 wt.% Na_2O in these reference materials plus plasma Ar.

Interferences can commonly be resolved analytically with the appropriate equipment, *e.g.,* higher mass resolution as available for some magnetic sector field instruments (*e.g.,* Moens *et al.* 1995) or dynamic reaction cell or collision cell ICP–MS technologies (*e.g.,* Tanner & Baranov 1999, Mason 2001). These techniques, offering advantages and new drawbacks in combination with laser ablation (*e.g.,* Shibuya *et al.* 1998, Hattendorf & Günther 2000, Latkoczy & Günther 2002), are beyond the scope of this chapter, and the reader is referred to the literature for more information. For multi-element fluid inclusion analysis, however, only a few contributions have been published using these instruments (*e.g.,* Günther *et al.* 2001, Allan *et al.* 2005). Note that operating high-resolution sector field instruments at high mass resolution results in a very substantial loss in sensitivity that may corrupt the anticipated benefit of the approach.

For multi-isotope elements where the presence of interferences on the isotope of choice for analysis cannot be excluded, test analyses recording more than one isotope of this element are a simple evaluation. For example, ^{95}Mo is about 1.6 times as abundant as ^{97}Mo, yet , ^{95}Mo may suffer from $(^{55}\text{Mn}^{40}\text{Ar})^+$ interference for the trace analysis of Mo in magmatic–hydrothermal fluids where MnO abundances may be several wt.%. Recording both ^{95}Mo and ^{97}Mo for a series of individual inclusion shots will then reveal whether the $(^{55}\text{Mn}^{40}\text{Ar})^+$ interference is relevant at the given ICP–MS operating conditions. It needs to be considered, however, that analyzing more than one isotope per element will decrease the duty cycle per element (*i.e.*, the time fraction per sweep spent for the measurement of a given analyte signal) and, thus, potentially deteriorate the analytical quality for short transient signals.

HOW TO SELECT, ANALYZE AND QUANTIFY A SERIES OF INDIVIDUAL FLUID INCLUSIONS

Having discussed fundamental parameters and aspects relevant for the analysis of individual, polyphase fluid inclusions, let us now focus on some practical aspects on how to perform such analyses and factors that should be taken into consideration during data reduction. Real data sets are used to assess figures of merit for fluid inclusion analysis.

Selection criteria for fluid inclusions suitable for LA–ICP–MS analysis

Sample preparation involves selection of "optimum" fluid inclusions from fluid inclusion assemblages (Figs. 12-1 and 12-5) for analysis. This is done prior to the laser ablation measurement session, and suitable inclusions are mapped so that they can be easily found for LA–ICP–MS analysis. Such fluid inclusions need to fulfill as many criteria as possible from the following list (see Fig. 12-5 for an example):

- Size should be between 5 and *ca.* 80 µm, preferably between 15 and 50 µm. Larger inclusions do not return higher signal to noise ratios, except for vapor inclusions, because the ablation rate is largely host mineral controlled; hence, LODs cannot be further lowered.
- Spherical inclusions (round, isometric shape) are best to maximize the inclusion signal size per unit time.
- Minimum depth should be *ca.* 20 µm (for small inclusions) to 40 µm (for large inclusions) to avoid surface contamination of the fluid inclusion signal (Fig. 12-3a).
- Maximum depth should not exceed *ca.* 60 µm. Signals from deeper inclusions tend to tail significantly, thereby reducing the signal to noise ratio and, consequently, returning elevated LODs. Moreover, there is the danger for ablation-induced element fractionation for such deep inclusions.
- Spatial isolation of individual inclusions is required, so that one selected inclusion can be ablated without liberating material from neighboring inclusions (Figs. 12-1b, 12-5).
- The sample section must be at least *ca.* 100 µm thick, preferably even thicker (*i.e.,* >3 times the depth of inclusions to be analyzed) to avoid inclusion rupture through the *lower* surface of the section. On the other hand, the section needs to be thin enough to allow for transmitted light inspection and localization of the fluid inclusions to be analyzed.

Among the above criteria, the minimum size of inclusions that may return useful data is most difficult to generalize. Important is the bulk dissolved load of these fluid inclusions; the more dilute the fluid is, the larger will be the minimal inclusion size for obtaining useful data. Because of the sequential data recording and the highly transient signal structure, only a few key elements can be determined reliably in very small inclusions. Shallow inclusions are not as suitable for analysis as they are prone to surface contamination and tend to explode. For a 10 µm inclusion at a preferred depth of >20 µm, the aspect ratio of the final ablation crater may easily exceed 3; hence, laser ablation-induced fractionation may become a problem. An increase in beam size is often not recommended because the mixed inclusion plus host signal may become dominated by host contribution, thus increasing the uncertainty on the determination of fluid element concentrations (Halter *et al.* 2002).

The technique of fluid inclusion ablation

Various techniques for improving the control on the fluid inclusion ablation process have been proposed, all aiming at the liberation of the entire fluid inclusion content without any losses, an endeavor which is far from trivial. In my view, the best technique for controlled ablation of the entire fluid inclusion content is **straight ablation**. In this

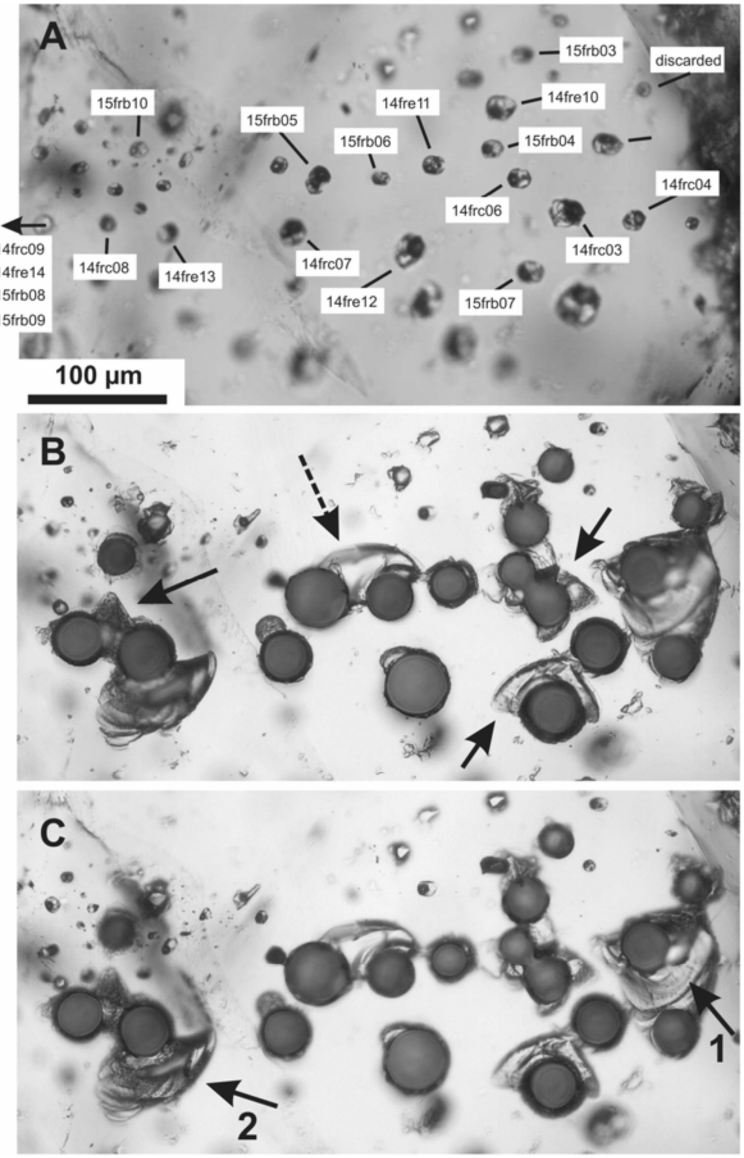

FIG. 12-5. **a)** Brine fluid inclusion assemblage, the LA–ICP–MS results of which are tabulated in Table 12-3. The labels are the shot numbers. The analysis of the shallow inclusion labeled "discarded" has not been saved because its signal contained surface contamination from previous ablations. Because of surface contamination resulting from deposits of ablated fluid inclusions, the sample has been surface-cleaned after the 14frc and 14fre shots and analyzed again the day after (*i.e.*, the 15frb series).
b) Same sample after the analyses, focused on the surface. Surficial breakout of quartz at crater rims occurred often on this sample (black arrows). In one case (dashed black arrow), a crack formed, but the quartz chip is still in place.
c) Same image as **b)** but focused 10 µm below the sample surface. Note that at a depth of 10 µm, all craters are round and sharply defined. Arrow 1 points to a deeper quartz breakout for shot 14frc05, causing loss of parts of the NaCl crystal (see text for explanation). This analysis has thus been rejected for average element concentration calculations (set in italics in Table 12-3). Arrow 2 indicates a similarly deep breakout of quartz. This analysis was a good one, however, because the analyzed fluid inclusion was deeper in the sample and thus not affected by this quartz breakout. Also note for **b)** and **c)** the inclusions near ablation pits may change their appearance without modifying their bulk chemical compositions (Lambrecht *et al.* 2008).

approach, the beam size is set to slightly larger than the maximum diameter of the fluid inclusion *before* the inclusion is opened, and the entire inclusion is then ablated at constant beam size (Fig. 12-3a). Admittedly, such an ablation procedure does not always work well, notably for quartz-hosted fluid inclusions or inclusions hosted by minerals possessing a good cleavage, where rupture of inclusions during ablation is sometimes observed. In order to minimize the uncontrolled release of liquid and daughter minerals, a stepwise procedure for opening fluid inclusions has been proposed, by which the fluid inclusion is pierced with a small crater size and, once open, the fluid inclusion is then ablated entirely by enlarging the beam size to slightly larger than the size of the fluid inclusion (Fig. 12-3b; see also Fig. 1 in Günther *et al.* 1998). This procedure indeed minimizes loss of inclusions due to rupturing but, unfortunately, has 3 serious drawbacks. First, a manually controlled crater size selection is required, yet most of the commercially available laser ablation systems are equipped with a motorized change in crater size that is too slow for the stepwise opening procedure. The next, more important drawback is surface contamination that inevitably will contaminate the fluid inclusion signal during stepwise opening. Figure 12-3a illustrates a signal from an inclusion of the assemblage illustrated in figure 12-5 obtained by fast manual stepwise opening to the final crater size *before* the inclusion is opened. The signals for some trace elements (*e.g.,* Pb, Na, and Cu) regularly observed at each beam size increase before the fluid inclusion is opened are real and represent surface contamination resulting in this case from previously ablated inclusions nearby. Surface contamination may also originate from material smeared during sample polishing, *e.g.*, sulfides or native gold intimately intergrown with the vein quartz. The latter often cannot be removed even by most careful cleaning with organic solvents or inorganic acids prior to laser-ablation analysis. One could envision using a few, low energy, large diameter cleaning laser pulses to remove surface contamination, but our experience has shown that even such low energy laser pulses may decrepitate inclusions. Surface cleaning shots generally work well for deeper inclusions (30–50 µm depth), but these inclusions can equally well be shot with a straight ablation procedure (with or without stepwise opening before the inclusion is hit) which itself avoids surface contamination for the fluid inclusion signal (Fig. 12-3a). Finally, every fluid inclusion has a confined mass that will be analyzed over a longer time interval when using the stepwise opening procedure. This will return lower signal to background intensity ratios that translate into elevated LODs when compared to straight ablation (as also acknowledged by Günther 2001). An elegant, custom-made approach for "stepwise" opening of crater size to final size has been presented by Guillong & Heinrich (2007b) who used an iris diaphragm with which ablation can be initiated at *ca.* 8 µm and the crater size increased fast and continuously to the final crater size to allow for straight ablation of the fluid inclusion.

Why rupture of fluid inclusions occurs, sometimes very often, during laser ablation cannot be answered satisfactorily to date. Processes contributing to the problem are:

1) Incomplete laser light absorbance by the host phase, allowing for energy transfer into the fluid inclusion (*e.g.,* Lambrecht *et al.* 2008), and even to the sample holder below (as already reported by Günther 2001). Consequently, inclusion contents are heated up and may partially or totally homogenize, resulting in an increased internal pressure. The transient signals obtained invariably from aqueo-carbonic fluid inclusions testify to this process (Fig. 12-3c, d).
2) Most of the inclusions analyzed in quartz formed in former cracks. It can be speculated that quartz precipitating during crack healing may have slightly different trace element compositions which may cause the quartz structure to be more prone to laser light-induced stress along healed fracture interfaces. During the analysis of quartz cements in our lab, cracking predominantly occurs along the interface between the detrital grain surface and the quartz cement.
3) Quartz may have a stressed mineral structure, for example as revealed by undulatory extinction. Experience shows that such quartz generally does not ablate as uniformly as non-stressed quartz.
4) For minerals with very good cleavage (*e.g.,* carbonates), the features alluded to above will more likely result in rupture of the fluid inclusion before it can be ablated in a controlled manner. Nonetheless, even fluid inclusions hosted by minerals with excellent cleavage such as calcite can be analyzed well (Bodnar, pers. comm. 2008). This illustrates that it is best practice to explore the ablation behavior of a given sample suite before engaging into extensive sample preparation for fluid inclusion analysis.

Active focusing (*e.g.,* Hirata & Nesbitt 1995) during fluid inclusion ablation also helps to ablate the entire fluid inclusion content completely. The laser beam optics of the GeoLas system are such that the laser beam imaged onto the sample surface is slightly conical. For this system, actively focusing the beam during laser ablation of fluid inclusions helps keeping the laser fluence on the ablation spot constant, minimizes deposition of inclusion material onto crater walls and will aid in completely sampling the fluid inclusion contents.

Representative recording of fast transient signals

Since the beginning of fluid inclusion analysis it has been observed that the external reproducibility of average element concentrations for fluid inclusion assemblages was conspicuously worse for some elements (notably some of the metals) when compared to classical "ionic" elements of the alkali and alkali-earth series such as Na, K, Rb, Sr or Cs. The external reproducibility of both these element groups for fluid inclusions is up to an order of magnitude worse than that typically achieved for the repetitive measurement of a homogeneous solid. Some of these poorly reproducible elements can actually be expected to reside in either the vapor bubble or in tiny precipitates (referred to as daughter crystals; *e.g.*,

Fig. 12-2b) that may be extremely enriched in rare elements. In fact, thermodynamic equilibrium modeling (McKibben 2007) predicts that many metals in solution at the time of fluid inclusion entrapment could be expected to precipitate when the fluid inclusion cools to ambient temperatures (unless these metals remain in solution in a metastable state). Tiny gold particles are one extreme example of such highly enriched daughter crystals. Signals produced from such small phases are highly transient, notably for fast washout ablation chambers as required for the analysis of inclusions in minerals at minimized LODs. Pettke *et al.* (2000b) have illustrated and discussed causes and effects of non-representative recording of fast transient signals by sequential analyte detection in detail. A key result of this work is that very fast recording protocols (10 ms dwell time per isotope is now commonly used) are required for multi-element fluid inclusion analysis. However, this compromises LODs because shorter dwell times (keeping all other parameters constant) translate into higher LODs (more below). Large volume aerosol transport systems would extend the signal produced from a given inclusion (recall that the mass for analysis is fixed), thereby maximizing representative recording of the transient signal and, potentially, allowing for longer dwell times. Importantly, however, it would also result in lower signal to noise ratios, translating into higher LODs. Signal smearing is therefore not considered to be a viable alternative for the analysis of commonly available fluid inclusion types.

To solve the above dilemma, Pettke & Klemm (in prep.) have developed what they call a "**jump routine**" where elements prone to occur as nuggets or in tiny precipitates in fluid inclusions are analyzed more often during one sweep than elements residing in solution (*e.g.,* the alkali and alkali-earth metals). The data-recording scheme follows the idea that the element prone to precipitation (in this example Au) is recorded every other time, resulting in a sweep sequence such as Na, Au, Si, Au, K, Au, Mn, Au, Fe, Au, Cu, Au, Sr, Au, Mo, Au, Pb, Au employed here. For this given example, the sweep time (one sequential measurement at 10 ms of all isotopes listed above; 3 ms quadrupole settling time) is 234 ms, of which Au is measured for 90 ms (9 times 10 ms). This results in a duty cycle for Au of 38.5%, significantly higher than the duty cycle of 7.7% achieved for the conventional Na, Si, K, Mn, Fe, Cu, Sr, Mo, Au, Pb routine at equal dwell times. More importantly, the maximum time elapsing without measuring for Au is reduced to 16 ms in the jump routine which strongly minimizes the likelihood of missing a significant fraction of a highly transient gold signal. Obviously, the probability of accurately recording the highly transient Au signal is dramatically improved when using the jump routine as opposed to the conventional routine where periods of 117 ms elapse without measuring for Au. This is impressively demonstrated in Table 12-3 by the uncertainties on average element concentrations for Mo and Au, both potentially precipitating elements in this sample. Although Mo is *ca.* 6000 times more abundant than Au, its external analytical uncertainty is only twice as good as that of Au. In fact, the analytical precision on the average Au concentration of this assemblage of 0.049 ± 0.015 µg g^{-1} (1 standard deviation) is remarkable for such a low content.

Sector field instruments provide a flat top peak and, therefore, would be much more appropriate for such a jump routine than a QMS with its slightly skewed Gaussian peak shape. However, data acquisition speed is limited by the still rather long (of the order of 50–100 ms) spectrometer settling time after a magnet field change. Therefore, unless the element of interest and the internal standard element required for signal quantification (more below) can be measured at one magnet setting, a sector field instrument will not be advantageous relative to fast quadrupole mass filters.

Signal quantification strategies

This section addresses the steps required to quantify element concentration data from instrument signal readouts obtained from the controlled ablation of an individual fluid inclusion, and addresses the inherent uncertainties. In brief, following representative data recording for the measurement of a series of individual fluid inclusions, signal quantification involves sequentially the following steps:

a) Integration of background interval and signal interval count rates for inclusion and pure host mineral sections for each analysis (Fig. 12-3), and background correction of inclusion and host signals
b) Subtraction of host mineral contribution from the inclusion signal
c) Drift correction based on the bracketing external standard measurements

d) Calculation of element concentration ratios based on the external standard
e) Conversion of these element concentration ratios into absolute element concentrations based on a known element concentration in the fluid inclusion
f) Filtering of the apparent element concentrations by the inclusion-specific LODs, to obtain the significant element concentration data for an individual fluid inclusion.

This procedure is identical to that described in Heinrich *et al.* (2003; summarized in their Fig. 10).

The basic relationship of LA–ICP–MS signal quantification (Longerich *et al.* 1996b) is

$$C_i(\mathrm{sam})/C_{IS}(\mathrm{sam}) = C_i(\mathrm{std})/C_{IS}(\mathrm{std}) * (I_i(\mathrm{sam})*I_{IS}(\mathrm{std}))/(I_{IS}(\mathrm{sam})*I_i(\mathrm{std})) * (S_i(\mathrm{sam})*S_{IS}(\mathrm{std}))/(S_{IS}(\mathrm{sam})*S_i(\mathrm{std})) \qquad (1)$$

where *C* is the concentration of the subscripted element *i* or internal standard *IS* in the material in brackets (*sam* is sample, *std* is external standard material), *I* refers to the background-corrected intensities (count rate; in counts per second, cps) and *S* denotes sensitivity. The sensitivity ratios $S_i(\mathrm{sam})/S_i(\mathrm{std})$ are identical for all elements including the IS element. Therefore, although $S_i(\mathrm{sam})/S_i(\mathrm{std})$ is unknown, the sensitivity term cancels, and the concentrations of all elements in the sample (C_i) can be calculated when $C_{IS}(\mathrm{sam})$ and the concentrations of all elements in the external standard ($C_i(\mathrm{std})$) are known.

We will now go from (a) through (f) in more detail. The raw count data are best read out from the instrument as counts per second (cps) because count rates already account for potentially different dwell times employed for analysis.

(a) Each measurement is ideally integrated for 3 signal intervals: gas background (prior to laser ablation), host mineral and inclusion plus host (Fig. 12-3). Each of these signal intervals needs to be filtered carefully for signal spikes. These are positive outliers, confined to one sweep and at least one order of magnitude larger than the neighboring count rates for this isotope. Signal spikes may originate from electronic spikes or, more likely, may represent a highly transient signal originating from a large (a few µm in size) particle flushed to the plasma that may be unrelated to the sample currently measured (*i.e.*, cross-contamination from previous ablations). Background-corrected count rates are now calculated for the host and the inclusion plus host signal intervals.

(b) The next step is subtraction of host mineral contribution from the mixed inclusion plus host signal. The mass proportions of pure host and pure inclusion in the mixed inclusion plus host signal are unknown *a priori*. The simplest approach for this host mineral correction is to assume that one element is exclusively present in the host mineral. For low-P fluid inclusions in quartz, Si is such an element. Element/Si count rate ratios are determined for the host mineral signal interval (*e.g.,* the host mineral possesses 10^{-5} cps Li normalized to one cps Si signal). The Si count rate in the inclusion plus host interval, assumed to originate exclusively from the host mineral ablated with the inclusion, is then multiplied by these element-specific host mineral count rate ratios to determine the total count rate of host mineral contribution. As an example let us assume we had 1000000 cps Si in our inclusion plus host signal interval. Having 10^{-5} cps Li per cps Si in the host mineral interval then translates into 10 cps Li host mineral contribution to the inclusion plus host signal interval, and these 10 cps Li are then subtracted from the inclusion plus host signal count rate for Li. This returns the host mineral-corrected count rate for Li, *i.e.*, the Li count rate of the pure inclusion signal. For the general case where all elements are variably present in both the host mineral and the inclusion, an iterative calculation scheme is required to deconvolve the mixed host plus inclusion signal into pure inclusion and pure host signal (Halter *et al.* 2002). Uncertainties resulting from host mineral correction have been discussed in great detail in Halter *et al.* (2002) who provided a rigorous mathematic uncertainty quantification for individual melt inclusions analyzed in bulk. These authors illustrated that for elements enriched in the host mineral, inclusion data are inevitably associated with a larger uncertainty, primarily resulting from host mineral correction of the analytical inclusion signal.

(c) The bracketing external standard measurements are then used to effect an instrumental drift correction using reference materials such as SRM 610 or SRM 612 from NIST. This results in an ablation-specific set of analyte sensitivities for the external standard (reference) material.

(d) The drift-corrected element sensitivities (*i.e.*, cps per µg g^{-1} element) calculated for each inclusion analysis individually are then used to derive element concentration ratios for the background- and host mineral-corrected fluid inclusion signals.

(e) Microthermometrically determined bulk salinity expressed as $NaCl_{equiv}$ may be used to derive the Na concentration in the fluid inclusion, by employing a "salt correction". This is a two step approach. (i) Element concentrations are calculated assuming that the $NaCl_{equiv}$ value is pure NaCl. This returns apparent concentrations for all other elements in the fluid inclusion, based on which one can identify those salt cations present in significant concentrations (*e.g.,* > 5% of the $NaCl_{equiv}$ value). (ii) Employ the empirical formulation for the salt correction discussed in Heinrich *et al.* (2003), to obtain "salt-corrected" element concentration data for the inclusion. This procedure corrects the microthermometrically determined $NaCl_{equiv}$ values for the presence of Cl-complexed cations other than Na. Heinrich *et al.* (2003) demonstrated that this correction scheme returns significantly more accurate element concentration data than would be obtained without accounting for the presence of metal chlorides other than NaCl when microthermometrically determined $NaCl_{equiv}$ values are used as the internal standard. Using microthermometrically determined Cl is an alternative internal standard. However, Cl measurement as a $^{35}Cl^+$ ion suffers from low sensitivity and polyatomic interference problems. We are currently exploring the quality of $^{35}Cl^+$ measurements by LA–ICP–MS using Cl bearing silicates. Future testing using synthetic fluid inclusions of known bulk Cl content will then reveal which approach of internal standardization (*i.e.,* Na or Cl as derived from microthermometry) returns more accurate results.

Heinrich *et al.* (2003) have convincingly demonstrated that neither absolute nor volume-normalized signal intensities have any direct relation to absolute element concentrations within individual fluid inclusions. Consequently, attempts to derive element concentration data without the use of an internal standard may not even provide the correct order of magnitude. It is also worth emphasizing that these highly transient fluid inclusion signals return element concentration data that are by no means erratic but that are externally well reproducible (see Table 12-3).

There are cases where accurate $NaCl_{equiv}$ data cannot be estimated from microthermometry, *e.g.,* for vapor-dominated inclusions where phase transitions in the aqueous phase cannot be observed reliably (*e.g.*, Fig. 12-2b), for CO_2-bearing inclusions that show clathrate melting in the absence of a free CO_2 phase, or for non-saline inclusions as can be produced in experiment (*e.g.*, Spandler *et al.* 2007). Here, an internal standard may be determined based on experimental data, *e.g.,* vapor salinities from the NaCl–H_2O phase diagram, or may be derived from element concentration data for the host mineral and experimental fluid–mineral element partition coefficients applicable to P and T of entrapment. Another approach chosen by Scambelluri *et al.* (2004) rests on mass balance considerations. These authors quantified the Li and B contents of antigorite dehydration fluid by estimating the bulk chlorinity of the dehydration fluid based on Cl contents of antigorite serpentinite and resulting dehydrated olivine–orthopyroxene rocks, and assuming that Na is exclusively present as NaCl in these fluid inclusions.

Note, importantly, that element concentration ratios of individual fluid inclusions are uniquely defined after having performed steps (a) to (d) above, *i.e.,* for cases where no reliable internal standard is available. For many geoscientific applications (*e.g.*, Landtwing *et al.* 2005, Klemm *et al.* 2007), these already are extremely useful data.

(f) Finally, the LODs are calculated for each element in every inclusion individually according to the formula (Longerich *et al.* 1996b)

$$\mathrm{LOD} = \frac{3 * \mathrm{stdev}\, \mathrm{I_i(bkg)}}{\mathrm{S_i} * \left(\frac{1}{\mathrm{N(bkg)}} + \frac{1}{\mathrm{N(an)}} \right)^{0.5}} \qquad (2)$$

where *stdev* stands for standard deviation, $I_i(bkg)$ refers to the intensity of the gas background for element *i*, S_i denotes the sensitivity of element *i* (as determined on the external standard), and *N* refers to the number of measurements (*i.e.,* sweeps) integrated for the background and analyte (*an*) signal interval, respectively. The above example returns the element concentration threshold value above which calculated element concentrations are real with 99% confidence.

Ways of improving on LODs

The LOD is a concentration threshold value above which a calculated concentration is deemed true, and this threshold value varies as a function of statistical parameters employed to derive it. For LA–ICP–MS signals, the variability of the background measurement around its mean intensity matters most (note the factor 3 in equation 2). The LODs are strongly element-dependent, because the analyzed isotopes are variably abundant in nature and instrument sensitivities vary greatly for different elements (*e.g.,* Table 12-2). High signal to background intensity ratios are also essential. The improvements in element sensitivities achieved through the use of H_2 in the aerosol carrier gas have been introduced above. The various parameters influencing the LODs specifically for fluid inclusion analysis are addressed now, and ways to optimize each of these in order to minimize LODs are highlighted. Importantly, improving LODs also improves the quality of low element concentration data, because analytical uncertainties stemming from counting statistics are reduced (more below).

For fluid inclusion analysis, a key parameter influencing the LODs is the shape of the transient signal produced from inclusion ablation. Since an individual fluid inclusion provides a confined mass for analysis, it is intuitive that the faster we drill though the entire inclusion and the faster we record it, the higher are the signal to background ratios for the analytes. Recall, however, that controlled and complete ablation of the fluid inclusion content must be ensured; catastrophic ablation, although fast, is no option. The aerosol transport system is also essential in that a slow washout will smear the transient fluid inclusion signal and thus lower its signal to noise ratios for the analytes. The aerosol transport system employed here has a washout time of *ca.* 3s which is well suited for fluid inclusion analysis (Fig. 12-3).

Moreover, given the confined mass of sample for fluid inclusion analysis, inclusion size, shape and depth in the sample add to the observed LOD variability between different inclusions. Spherical inclusions are best, and an optimum depth is between *ca.* 20 and 50 µm (shallower for smaller inclusions) to allow for straight ablation. The stepwise opening signal shown in Fig. 12-3b has been modeled as a straight ablation signal (not shown), for which the LODs are improved by up to *ca.* 35%; hence, it is obvious that stepwise opening should be avoided also when optimizing LODs.

The fluid inclusion bulk salinity is also important, because the more dilute the fluid in the inclusion (fluid inclusion salinity in nature varies by more than two orders of magnitude) the greater is the fraction of H_2O or CO_2, and these pass by unmeasured. As can be seen from Fig. 12-3, controlled ablation of a fluid inclusion produces a signal the transient shape of which is largely controlled by the laser ablation rate of the host mineral that determines the speed with which laser ablation drills "through the inclusion". Consequently, dilute fluid inclusions simply provide less analytes per unit time. This lowers the signal to noise ratio, translating into elevated LODs. The fact that the ablation rate of a fluid inclusion is largely controlled by the ablation rate of the host mineral for controlled inclusion ablation also explains why inclusions larger than about 50 µm will not result in improved LODs (except for vapor inclusions).

The fluid inclusion bulk density affects the LODs in a way similar to that of bulk salinity. The bulk density for aqueous inclusions determines the fraction of the entire fluid inclusion that is liquid at room temperature. For a vapor inclusion the liquid fraction may be for example 5%, and even if the salinity of this liquid is high, the total mass of solutes for this inclusion will be low. Consequently, LODs are elevated. In other words, a dense, spherical fluid inclusion of 20 µm diameter containing 50 wt.% NaCl equivalent has about 2 ng material that can be analyzed. The best LODs obtained for such inclusions in a multi-element menu is *ca.* 0.01 $\mu g\ g^{-1}$, translating into 0.05 fg required for the significant analysis of such well detectable elements. In my experience, best LODs can be achieved for *ca.* 30 µm spherical fluid inclusions about 30 µm beneath the sample surface using straight ablation.

Next, the dwell time affects the LOD significantly. Increasing the dwell time reduces the variability of the background measurement around its mean; hence, LODs are lowered according to equation 2 above. For fluid inclusion analysis, however, an increase in dwell times deteriorates the temporal resolution of the fast transient signal to the point where representative recording in sequential mode may no longer be possible (addressed above). It is here, where the jump routine provides an additional benefit. Not only does the jump routine ensure representative sampling of the jumped analyte, it also increases significantly its dwell time per sweep. For our example, Au has a summed dwell time of 90 ms per sweep. With this long dwell time, the standard deviation of the background count rate for Au improved by about a factor of 4, and this significantly reduces the resulting LOD. Thanks to this additional benefit of the jump routine, the significant quantification of Au in the example reported in Table 12-3 has become possible.

Sometimes, a short, tiny but significant signal identified graphically (*e.g.,* Fig. 12-3b) may not survive LOD filtering, because treating this short, tiny signal using average count rates as determined across the entire signal interval (defined based on *e.g.,* Na) will "dilute" this short, tiny signal to the point that it may no longer survive the >99% confidence filtering. For such signals, a semi-quantitative concentration can be derived by relaxing the statistical limit for the LOD from 3 SD_{bkg} to 2 or 1 SD_{bkg} (referred to as the limit of quantification by Günther *et al.* 1998).

Finally, LODs are useful numbers only when reported for known LA–ICP–MS parameters, fluid inclusion size, bulk density and bulk salinity, and LOD filtering criteria employed.

PRECISE AND ACCURATE ISOTOPE RATIO MEASUREMENTS USING LA–MC–ICP–MS: ACHIEVEMENTS AND PROSPECTS

Constraints on the source of fluids help identify provenance of components, thus constraining processes of chemical and heat transfer in the Earth. A prime tool for this is radiogenic isotopes, notably because different sources often possess quite variable signatures and, for heavier isotopes, mass-dependent fractionation during geological processes does not modify the isotopic signatures (unlike for classical light stable isotopes, *e.g.,* H, C, O, Li, B). Therefore, accurate data at moderate precision may often resolve potential source components. Pettke *et al.* (2003) reported a reconnaissance study measuring Pb isotope ratios in individual fluid inclusions using laser ablation–multiple collector–ICP–MS (LA–MC–ICP–MS). The precision achieved in this study exceeded that obtainable with single-collector instruments, motivating a more in depth evaluation of this technique. Today, accurate Pb isotope data including quantification of mass 204 can be obtained with 2 SD uncertainties on inclusion to inclusion reproducibility from assemblages of 0.05 ($^{208}Pb/^{206}Pb$ and $^{207}Pb/^{206}Pb$ ratios) and 0.4% (Pb isotope ratios normalized to mass 204), respectively (Fig. 12-6; Pettke *et al.* 2008). Natural fluid inclusions that contain more Pb and are larger than those analyzed in figure 12-6 can be measured even more precisely for Pb isotope ratios normalized to mass 204, achieving 0.15% 2 SD uncertainties. This section briefly summarizes the key aspects of this method development.

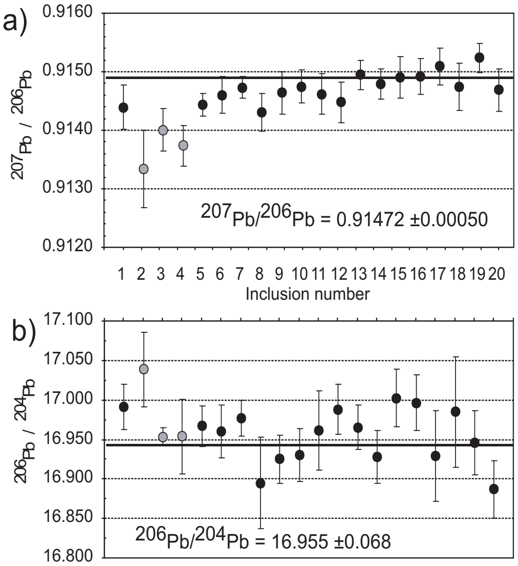

FIG. 12-6. External reproducibility of Pb isotope ratio determinations of individual synthetic fluid inclusions, with an external uncertainty quoted at the 2 SD level, **a)** for $^{207}Pb/^{206}Pb$ ratios and **b)** for $^{206}Pb/^{204}Pb$ ratios. The thick solid line represents the SRM 981 Pb isotope reference value (Baker *et al.* 2004). The three grey data points are deemed outliers (due to poorly controlled ablation; inclusion number 3 even exploded) and are thus not used for statistics. Note that the uncertainty for the example shown in Fig. 12-6b is higher than that quoted in text because the synthetic fluid inclusions have lower Pb concentrations than some of the natural inclusions we have analyzed so far.

All data have been acquired with a GeoLas 193 nm ArF excimer laser system combined with either the Nu Plasma or the Nu Plasma 1700 MC–ICP–MS instruments (for machine parameters see Pettke *et al.*, in prep.). Self-made synthetic fluid inclusions of known Pb isotopic compositions (SRM 981 from NIST) have been used to establish the LA–MC–ICP–MS analytical protocol for fast transient signals as produced from the ablation of individual fluid inclusions. These inclusions contained *ca.* 5000 µg g^{-1} Pb which compares well with Pb concentrations typically measured in magmatic–hydrothermal brine inclusions (*e.g.,* Audétat *et al.* 2000, Landtwing *et al.* 2005, Klemm *et al.* 2007). For an egg-shaped fluid inclusion with longest dimension of 30 µm, the amount of Pb available for analysis is of the order of 0.3 ng. This is considerably less than the amounts consumed for precise MC–ICP–MS isotope analysis of Pb in solution mode (isotopic ratios of ±100 ppm precision can be obtained on amounts of Pb as low as *ca.* 5–10 ng; Baker *et al.* 2004).

Controlled ablation of individual fluid inclusions ensured, masses 200, 202, 203, 204, 205, 206, 207 and 208 were recorded simultaneously on Faraday detectors and read out in 0.2 s intervals (sweeps), employing the instrument's transient software capabilities (Fig. 12-7). Since Pb does not possess a stable isotope pair, Tl was admixed via desolvated nebulisation to the LA aerosol up-torch

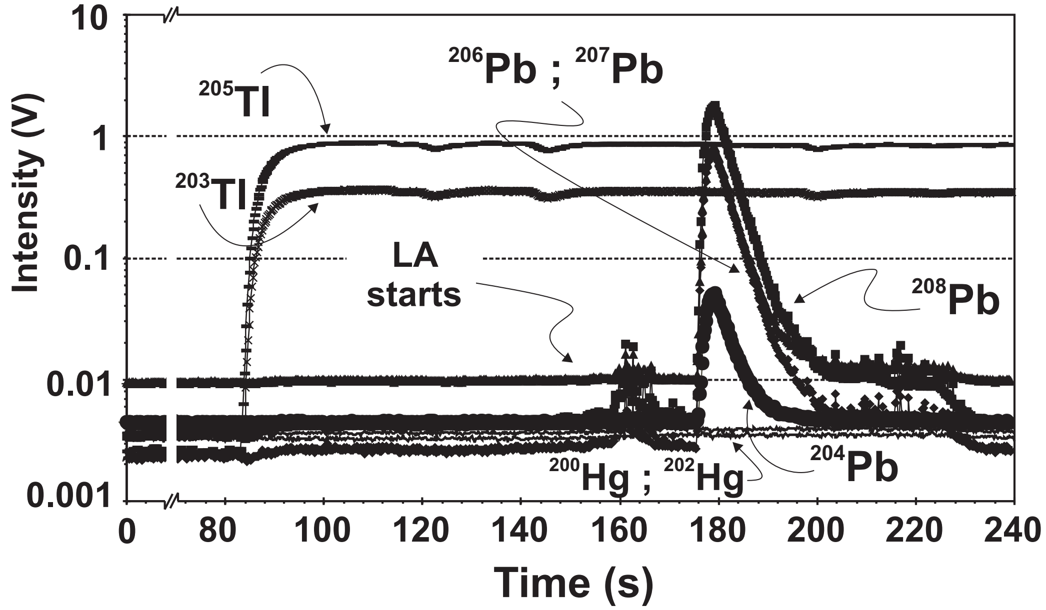

FIG. 12-7. Transient Pb isotope signal of a synthetic fluid inclusion. The Tl signal rising before laser ablation (LA) starts is from a desolvated Tl solution and is used for within-run mass bias correction. Once the Tl signal is stable, the laser ablation starts, and ablation of the fluid inclusion superimposes a Pb signal onto the Tl signal. Note that for quartz-hosted fluid inclusions, a host mineral correction is not required for Pb isotopic ratio analysis since quartz contains virtually no Pb.

for use in within-run correction of mass bias (*e.g.,* Longerich *et al.* 1987). Raw data have been corrected for background contributions first (gas background measured on peak prior to laser ablation). Background-corrected intensities were corrected for interferences, of which ^{204}Hg on ^{204}Pb was the only significant one. The measured ^{205}Tl/^{203}Tl isotope ratio was used to predict the mass-biased ^{202}Hg/^{204}Hg ratio of interfering mercury, and the ^{204}Hg on ^{204}Pb interference was corrected successfully this way. Other interferences have been shown to be insignificant at the analytical accuracy obtained, even on SRM 610 glass. These Hg interference-corrected Pb isotope ratios were then corrected for mass bias based on the within-run measured ^{205}Tl/^{203}Tl using procedures of Woodhead (2002) and Baxter *et al.* (2006). For more details and justification of this procedure, the reader is referred to Pettke *et al.* (in prep.). The 2 SD uncertainty on the external reproducibility of SRM 610 ablations during a one day analytical session converged to ± 130 ppm for ^{208}Pb/^{206}Pb and ^{207}Pb/^{206}Pb ratios and to ± 420 ppm for Pb isotope ratios normalized to mass 204, or ± 22 and ± 73 ppm, respectively, at the 2 SE uncertainty level (n=36), irrespective of whether line scan or single spot ablations (90 µm crater size) were acquired.

Detailed inspection of the transient fluid inclusion signals revealed evolving isotope ratios that are ascribed to fractionation occuring during the process of fluid inclusion ablation (Pettke *et al.* (in prep.). This fractionation does not affect analytical accuracy, however, given controlled ablation of the entire fluid inclusion and integration of the entire transient signal.

Magmatic–hydrothermal fluid inclusions typically contain a few to several thousand µg g^{-1} Pb (Table 12-3), translating into about 0.2–1 ng of Pb available for the analysis of individual ellipsoidal inclusions 40x40x30 µm in size. Acceptably reproducible results (±1 ‰ and 5 ‰, respectively) were obtained for inclusions containing as little as 0.1 ng Pb with the current setup using Faraday detectors, demonstrating the potential of our analytical protocol for low amount fast transient signals.

FIGURES OF MERIT

The type of geochemical problem defines the type and precision of the data set required to resolve the issues. More importantly, it is the statistics employed that influence the analytical uncertainty cited on a given measurement, and it is crucial to define which contributions are relevant when determining an overall analytical uncertainty. Finally, the data-recording scheme (*e.g.,* multiple collector *vs.* single collector data recording) also significantly influences which statistical parameters are most relevant.

Analytical precision

For LA–ICP–MS analysis in general, two fundamentally different results are obtained:

a) The analytical uncertainty associated with data obtained for an individual analysis is referred to as internal or within-run or shot precision.
b) The uncertainty obtained on the average of a series of individual analyses of a homogeneous material (*e.g.,* a series of fluid inclusions from a homogeneously entrapped assemblage), is referred to as external or run-to-run or shot-to-shot precision or, specifically, inclusion-to-inclusion precision.

LA–ICP–MS analysis of fluid inclusions inevitably produces highly transient signals (Figs. 12-3 and 12-7), a signal structure that is explicitly avoided in all other *in situ* analytical techniques. For the analysis of a series of fluid inclusions belonging to a fluid inclusion assemblage, the following considerations are thus relevant:

(a) Internal precision: The assessment of the analytical uncertainty for element concentration data of individual fluid inclusions acquired by sequential data recording (*i.e.,* single collector instruments) is extremely difficult because several contributions – interrelated or independent – contribute to the overall uncertainty. Among all these, important contributions are:

- Counting statistics uncertainties, which are especially important for low intensity signals.
- Variability in signal intensities within the transient signal interval (Fig. 12-3).

While the former uncertainty can be calculated from data acquired, the latter is impossible to quantify for fast transient signals as produced from fluid inclusion ablation. Moreover, analytical uncertainties stemming from systematic contributions (*e.g.,* short term variability resulting from plasma flicker) are not considered here. Consequently, if there is an uncertainty on individual fluid inclusion analysis to be reported, then it is a minimum uncertainty provided by counting statistics that dominates the overall internal precision unless instrumental background intensities are large.

For the determination of isotope ratios by simultaneous measurements as provided by multiple collector instruments, common use is to calculate the final isotope ratios for each sweep (*i.e.,* time slice or data readout) and then calculate the variability around the mean (*i.e.,* the standard error of the mean) isotope ratio for the entire analyte signal. While this procedure is robust for signals of constant intensity (because each sweep is measured with equal precision), it may not be the method of choice for fast transient signals from fluid inclusions (Fig. 12-7). Examining figure 12-7 it appears intuitive that an average weighted on the basis of signal intensities per sweep would probably be a better representation of the average isotope ratios measured for an inclusion signal. Therefore, the Pb isotope data set of 20 fluid inclusions has been reduced in two modes (Pettke *et al.*, in prep.):

i) The Pb isotope ratios have been calculated based on corrected signal intensities for each sweep individually, and the final result corresponds to the mean of the sweeps in the signal.
ii) The isotope ratio has been calculated based on the corrected isotope intensities summed across the entire signal interval.

While each reading (sweep) is weighed equally in approach (i), irrespective of signal intensity, the high intensity readings are more significant in defining the average Pb isotope ratio of an individual fluid inclusion in approach (ii). Indeed, the external reproducibility obtained for data reduced in mode (ii) is better (Pettke *et al.*, in prep.), thus illustrating the effect of overrating the low intensity measurements near the signal tails in mode (i). This result illustrates that intensity-weighted mean data more accurately determine the isotope ratios of fast transient signals measured by MC–ICP–MS.

(b) External precision is a much more robust assessment of the overall analytical reproducibility, for both single and multiple collector data recordings. The external precision is best determined for fluid inclusions belonging to compositionally homogeneous assemblages (Figs. 12-1 and 12-5). Such an external reproducibility can be obtained by calculating either simple averages and associated uncertainties (*i.e.,* individual inclusion analyses are weighted equally), or uncertainty-weighted averages (where precise determinations exert a larger influence on the average concentrations than do imprecise determinations; see Pettke *et al.* 2004 for an example). Uncertainty-weighted average data sets are preferred notably for element concentrations close to their LODs, because such concentrations have grossly variable analytical precisions primarily resulting from counting statistics. The current example of 20 fluid inclusions analyzed for element concentrations individually (Table 12-3) demonstrates that for elements residing dominantly in the aqueous solution during analysis, external uncertainties on average element concentration data of ±5% (1 standard deviation) can be achieved (in this case, all elements except Au are far above their respective LODs, rendering an uncertainty-weighted averaging based on counting statistics uncertainties unnecessary). Such precise data demonstrate that these inclusions indeed represent individual samples of a compositionally uniform fluid, and that their individual LA–ICP–MS analysis was controlled and complete. Table 12-3 also reports one fluid inclusion analysis (14frc05, set in italics; see also Fig. 12-5) that has not been used for average data calculation. This inclusion reveals a deficit in Na and excesses in all other major cation concentrations, which is indicative of loss of at least some of the NaCl daughter crystal during analysis (given microthermometric uniformity of analyzed inclusions). If this occurs, signal intensity ratios of element/Na are elevated, however, the signal of Na is equaled to the internal standard element concentration during data reduction, and this returns excesses for those elements completely sampled during analysis. This example demonstrates that average fluid element concentrations determined for fluid inclusion assemblages (homogeneous entrapment) provide the most accurate data, notably also because outliers can be identified and excluded from further consideration (as already stressed by Pettke *et al.* 2004).

The external uncertainty of data obtained for a fluid inclusion assemblage (homogeneous entrapment) could also be expressed as the standard error of the mean of N analyses, *i.e.,* the variability of data around the mean value. This method of uncertainty quantification returns lower values when compared to the standard deviation because the standard deviation is divided by the square root of N analyses to obtain the standard error of the mean. For our example of 20 inclusions in Table 12-3, it can be seen that the standard error of the mean is a factor of 4–5 lower than the corresponding standard deviation. It is thus essential that the type of uncertainty cited is defined.

Analytical accuracy

Analytical accuracy is best demonstrated through the analysis of synthetic fluid inclusions of known composition or by analyzing a fluid inclusion assemblage using various, independent analytical techniques. Extensive tests demonstrate that accurate fluid inclusion compositional (Heinrich *et al.* 2003, Allan *et al.* 2005) and Pb isotopic (Pettke *et al.* 2008) data can be obtained at useful precision.

First of all, representative and complete sampling and signal recording of the content of individual fluid inclusions is a prerequisite for potentially obtaining accurate data – this is why I put so much emphasis on these issues above. The best indication for the absence of such analytical problems for fluid inclusions of unknown composition is the quality of the external reproducibility obtained for assemblages. The data reported in Table 12-3, by themselves, document this.

Accuracy to date is limited most significantly by the accuracy with which the concentration of the internal standard element can be derived, *e.g.,* from microthermometric data, as documented in Heinrich *et al.* (2003). These authors concluded that the farther the bulk fluid composition deviates from the binary H_2O–NaCl system, the larger is the probable error associated with the determination of the Na concentration to be used as the internal standard element.

It is also obvious that the quality with which the IS signal is recorded directly translates on all element concentrations calculated based on this IS. This is nicely demonstrated for the inclusion analysis 14frc05 (Table 12-3) discussed above, where a part of the NaCl daughter crystal has been lost during analysis. This also implies that the use of Cl for internal standardization is limited to relatively high fluid salinities, since the low sensitivity of Cl^+ plus the elevated background on mass 35 will return high enough signal to noise ratios for calibration only for high fluid Cl concentrations. Moreover, our own tests (unpublished data) have revealed serious interference problems on mass 35 notably at low signal intensities, the exact nature of which is currently under investigation.

For fluids that contain significant amounts of non-chlorine complexed species (*e.g.,* sulfuric or fluoro- or hydrated silicate species) the use of an internal standard other than microthermometrically determined Na concentration may be preferable. It is here where much progress in the accuracy of signal quantification for fluid inclusions can be expected in the near future.

Recall that the analytical accuracy on element concentration ratios is uniquely defined by the use of external standardization alone (plus all instrument-related uncertainty contributions). As a consequence, analytical accuracy on element concentration ratios will be limited at least for some elements by the accuracy with which these element concentrations are known for the external standard material employed for analysis (*e.g.,* SRM 612 and SRM 610 glasses in our case). In fact, some of the relevant fluid elements are only poorly constrained in the SRM 61X glasses, and some of the most commonly used values are demonstrably wrong (for a detailed assessment see Spandler *et al.* 2008, and in prep.; Jochum 2008).

Note that when averaging individual fluid inclusion data from assemblages, there may be a bias towards elevated element concentrations for elements near their LOD, because analyses below the LOD are obviously omitted for averaging. In such cases, the average element concentration data should be regarded as maximum element concentrations.

In summary, the most severe limitation for LA–ICP–MS inclusion analysis is the knowledge of the absolutely necessary internal standard constraint. This is most commonly an element concentration, but for some applications it can also be an element concentration ratio (*e.g.,* Halter *et al.* 2002, Pettke 2006). For aqueous fluid inclusions, a more accurate multi-component description of the liquidus surface of ice and the final dissolution of hydrohalite or halite would be highly desirable, but equations of state for fluids with >3 components have so far not been derived. The data presented here demonstrate that a LA–ICP–MS analytical setup dedicated for the analysis of inclusions in minerals can provide data at an external precision that may well exceed the accuracy currently achievable for element concentration data.

ACKNOWLEDGEMENTS

I would like to thank Carl Spandler and Janos Kodolanyi for sharing their time and experience on our new LA–ICP–MS facility and the many interesting and stimulating ideas and discussions on LA–ICP–MS issues. In the group of Chris Heinrich at ETHZ I had great opportunities and ample exposure to excellent LA–ICP–MS fluid inclusion projects for which I am very grateful to you, Chris. Leonhard Klemm kindly provided the sample GI-13-17 that he originally received from Steve Kesler. I also thank Detlef Günther for many great contributions he made to the topic I cover here. I am indebted to Bob Bodnar and Paul Mason for very helpful reviews, allowing me to refine some of my statements, and to Paul Sylvester for his efforts in editorial handling. Continued funding by the Swiss National Science Foundation (current project PP002–106569) and funding of a LA–ICP–MS technical upgrade by the Berne University Research Foundation are greatly acknowledged.

REFERENCES

ALLAN, M.M., YARDLEY, B.W.D., FORBES, L.J., SHMULOVICH, K.I., BANKS, D.A. & SHEPHERD, T.J. (2005): Validation of LA–ICP–MS fluid inclusion analysis with synthetic fluid inclusions. *Am. Mineral.* **90**, 1767-1775.

AUDÉTAT, A. & GÜNTHER, D. (1999): Mobility and H_2O loss from fluid inclusions in natural quartz crystals. *Contrib. Min. Petrol.* **137**, 1-14.

AUDÉTAT, A. & PETTKE, T. (2003): The magmatic–hydrothermal evolution of two barren granites: A melt and fluid inclusion study of the Rito del Medio and Canada Pinabete plutons in northern New Mexico (USA). *Geochim. Cosmochim. Acta* **67**, 97-121.

AUDÉTAT, A., GÜNTHER, D. & HEINRICH, C.A. (1998): Formation of a magmatic–hydrothermal ore deposit: Insights with LA–ICP–MS analysis of fluid inclusions. *Science* **279**, 2091-2094.

AUDÉTAT, A., GÜNTHER, D. & HEINRICH, C.A. (2000): Magmatic–hydrothermal evolution in a fractionating granite: A microchemical study of the Sn–W–F-mineralized Mole Granite (Australia). *Geochim. Cosmochim. Acta* **64**, 3373-3393.

BAKER, J., PEATE, D., WAIGHT, T. & MEYZEN, C. (2004): Pb isotopic analysis of standards and samples using a ^{207}Pb–^{204}Pb double spike and thallium to correct for mass bias with a double-focusing MC–ICP–MS. *Chem. Geol.* **211**, 275-303.

BANKS, D.A., DAVIES, G.R., YARDLEY, B.W.D., MCCAIG, A.M. & GRANT, N.T. (1991): The chemistry of brines from an Alpine thrust system in the Central Pyrenees: An application of fluid inclusion analysis to the study of fluid behaviour in orogenesis. *Geochim. Cosmochim. Acta* **55**, 1021-1030.

BANKS, D.A., RICE, C., STEELE, G., BOYCE, A. & FALLICK, T. (2007): The formation of the world's largest silver deposit, Cerro Rico, Bolivia. Abstract. Biennial Conference ECROFI XIX, Bern, Switzerland, 17-20 July, p. 72.

BAXTER, D.C., RODUSHKIN, I., ENGSTROM, E. & MALINOVSKY, D. (2006): Revised exponential model for mass bias correction using an internal standard for isotope abundance ratio measurements by multi-collector inductively coupled plasma mass spectrometry. *J. Analyt. Atom. Spectrom.* **21**(4), 427-430.

BENNETT, J.N. & GRANT, J.N. (1980): Analysis of fluid inclusions using a pulsed laser micro-probe. *Mineral. Mag.* **43**, 945-947.

BODNAR, R.J. (2003): Reequilibration of fluid inclusions. *In* Fluid inclusions: Analysis and data interpretation (I. Samson, A. Anderson & D. Marshall, eds.). *Mineral. Assoc. Can. Short Course Series Volume* **32**, 213-231.

BODNAR, R.J. & STUDENT, J.J. (2006): Melt inclusions in plutonic rocks: petrography and microthermometry. *In* Melt Inclusions in Plutonic Rocks (J. D. Webster, ed.). *Mineral. Assoc. Can. Short Course Series Volume* **36**, 1-25.

BOIRON M.C., DUBESSY J., ANDRE N., BRIAND A., LACOUR J.L., MAUCHIEN P. & MERMET J.M. (1991): Analysis of mono-atomic ions in individual fluid inclusions by laser-produced plasma emission-spectroscopy. *Geochim. Cosmochim. Acta* **55**, 917-923.

BOTTRELL, S.H., YARDLEY, B.W.D. & BUCKLEY, F. (1988): A modified crush-leach method for the analysis of fluid inclusion electrolytes. *Bull. Minéral.* **111**, 279-290.

CZAMANSKE, G.K., ROEDDER, E. & BURNS, F.C. (1963): Neutron activation analysis of fluid inclusions for copper, manganese, and zinc. *Science* **140**, 401-403.

DELOULE, E. & ELOY, J.F. (1982): Improvements of laser probe mass-spectrometry for the chemical analysis of fluid inclusions in ores. *Chem. Geol.* **37**, 191-202.

DIAMOND, L.W. (1990): Fluid inclusion evidence for P–V–T–X evolution of hydrothermal solutions in late-Alpine gold–quartz veins at Brusson, northwest Italian Alps. *Am. J. Sci.* **290**, 912-958.

DIAMOND, L.W., JACKMAN, J.A. & CHAROY, B. (1991): Cation ratios of fluid inclusions in a gold–quartz vein at Brusson, Val d'Ayas, northwestern Italian Alps: Comparison of bulk crush-leach results with SIMS analyses of individual inclusions. *Chem. Geol.* **90**, 71-78.

DUC-TIN, Q., AUDÉTAT, A. & KEPPLER, H. (2007): Solubility of tin in (Cl, F)-bearing aqueous fluids at 700 degrees C, 140 MPa: A LA–ICP–MS study on synthetic fluid inclusions. *Geochim. Cosmochim. Acta* **71**, 3323-3335.

EGGINS, S.M., KINSLEY, L.P.J. & SHELLEY, J.M.G. (1998): Deposition and element fractionation processes during atmospheric pressure laser sampling for analysis by ICP–MS. *Applied Surface Science* **129**, 278-286.

EGGINS, S.M., DE DECKKER, P. & MARSHALL, J. (2003): Mg/Ca variation in planktonic foraminifera tests: implications for reconstructing palaeo-seawater temperature and habitat migration. *Earth Planet. Sci. Lett.* **212**, 291-306.

FRYER, B.J., JACKSON, S.E. & LONGERICH, H.P. (1995): Design, operation and role of the laser-ablation microprobe coupled with an inductively-coupled plasma–mass-spectrometer (LAM–ICP–MS) in the Earth sciences. *Can. Mineral.* **33**, 303-312.

GOLDSTEIN R.H. & REYNOLDS T.J. (1994): Systematics of fluid inclusions in diagenetic minerals. *Society for Sedimentary Geology Short Course* **31**, 199p.

GUILLONG, M. & GÜNTHER, D. (2002): Effect of particle size distribution on ICP-induced elemental fractionation in laser ablation-inductively coupled plasma–mass spectrometry. *J. Analyt. Atom. Spectrom.* **17**, 831-837.

GUILLONG, M. & HEINRICH, C.A. (2007a): Sensitivity enhancement in laser ablation ICP–MS using small amounts of hydrogen in the carrier gas. *J. Anal. At. Spectrom.* **22**, 1488-1494.

GUILLONG, M. & HEINRICH, C.A. (2007b): LA–ICP–MS analysis of inclusions: Improved ablation and detection. Biennial Conference ECROFI XIX, Bern, Switzerland, 17-20 July, p. 82.

GÜNTHER, D. (2001): Quantitative fluid inclusion analysis using a 193 nm excimer laser-ablation system coupled to ICP–MS. *In* Laser Ablation in the Earth Sciences (P. Sylvester, ed.). *Minera.l Assoc. Canada Short Course Series Volume* **29**, 47-62.

GÜNTHER, D. & HATTENDORF, B. (2005): Solid sample analysis using laser ablation inductively coupled plasma mass spectrometry. *TRAC - Trends in Analytical Chemistry* **24**, 255-265.

GÜNTHER, D. & HEINRICH, C.A. (1999): Enhanced sensitivity in laser ablation-ICP mass spectrometry using helium-argon mixtures as aerosol carrier – plenary lecture. *J. Analyt. Atom. Spectrom.* **14**, 1363-1368.

GÜNTHER, D., FRISCHKNECHT, R., HEINRICH, C.A. & KAHLERT, H.J. (1997): Capabilities of an Argon Fluoride 193 nm excimer laser for laser ablation inductively coupled plasma mass spectrometry microanalysis of geological materials. *J. Analyt. Atom. Spectrom.* **12**, 939-944.

GÜNTHER, D., AUDÉTAT, A., FRISCHKNECHT, R. & HEINRICH, C.A. (1998): Quantitative analysis of major, minor and trace elements in fluid inclusions using laser ablation inductively coupled plasma mass spectrometry. *J. Analyt. Atom. Spectrom.* **13**, 263-270.

GÜNTHER, D., HATTENDORF, B. & AUDÉTAT, A. (2001): Multi-element analysis of melt and fluid inclusions with improved detection capabilities for Ca and Fe using laser ablation with a dynamic reaction cell ICP–MS. *J. Analyt. Atom. Spectrom.* **16**, 1085-1090.

HALTER, W.E., PETTKE, T., HEINRICH, C.A. & ROTHEN-RUTISHAUSER, B. (2002): Major to trace element analysis of melt inclusions by laser-ablation ICP–MS: methods of quantification. *Chem. Geol.* **183**, 63-86.

HALTER, W.E., PETTKE, T. & HEINRICH, C.A. (2004): Laser-ablation ICP–MS analysis of silicate and sulfide melt inclusions in an andesitic complex I: analytical approach and data evaluation. *Contrib. Min. Petrol.* **147**, 385-396.

HANLEY, J.J., MUNGALL, J.E., PETTKE, T., SPOONER, E.T.C. & BRAY, C.J. (2005a): Ore metal redistribution by hydrocarbon–brine and hydrocarbon–halide melt phases, North Range footwall of the Sudbury Igneous Complex, Ontario, Canada. *Mineralium Deposita* **40**, 237-256.

HANLEY, J.J., PETTKE, T., MUNGALL, J.E. & SPOONER, E.T.C. (2005b): The solubility of platinum and gold in NaCl brines at 1.5 kbar, 600 to 800 degrees C: A laser ablation ICP–MS pilot study of synthetic fluid inclusions. *Geochim. Cosmochim. Acta* **69**(10), 2593-2611.

HATTENDORF, B. & GÜNTHER, D. (2000): Characteristics and capabilities of an ICP–MS with a dynamic reaction cell for dry aerosols and laser ablation. *J. Analyt. Atom. Spectrom.* **15**, 1125-1131.

HEINRICH C.A., GÜNTHER D., AUDETAT A., ULRICH T., & FRISCHKNECHT R. (1999): Metal fractionation between magmatic brine and vapor, determined by microanalysis of fluid inclusions. *Geology* **27**, 755-758.

HEINRICH, C.A., PETTKE, T., HALTER, W.E., AIGNER-TORRES, M., AUDÉTAT, A., GÜNTHER, D., HATTENDORF, B., BLEINER, D., GUILLONG, M. & HORN, I. (2003): Quantitative multi-element analysis of minerals, fluid and melt inclusions by laser-ablation inductively-coupled-plasma mass-spectrometry. *Geochim. Cosmochim. Acta* **67**, 3473-3497.

HIRATA, T. & NESBITT, R.W. (1995): U–Pb isotope geochronology of zircon – evaluation of the laser probe-inductively coupled plasma-mass spectrometry technique. *Geochim. Cosmochim. Acta* **59**, 2491-2500.

HORN, E.E. & TRAXEL, K. (1987): Investigations of individual fluid inclusions with the Heidelberg proton microprobe – A nondestructive analytical method. *Chem. Geol.* **61**, 29-35.

JACKSON, S.E., LONGERICH, H.P., DUNNING, G.R. & FRYER, B.J. (1992): The application of laser-ablation microprobe – inductively coupled plasma – mass-spectrometry (LAM–ICP–MS) to in situ trace-element determinations in minerals. *Can. Mineral.* **30**, 1049-1064.

JOCHUM, K.P. & STOLL, B. (2008): Reference materials for elemental and isotopic analyses by LA–(MC)–ICP–MS: successes and outstanding needs. *In* Laser Ablation ICP–MS in the Earth Sciences: Current Practices and Outstanding Issues (P. Sylvester, *ed.*). *Mineral. Assoc. Can. Short Course Series* **40**, 147-168.

KESSEL, R., ULMER, P., PETTKE, T., SCHMIDT, M.W. & THOMPSON, A.B. (2005): The water–basalt system at 4 to 6 GPa: Phase relations and second critical endpoint in a K-free eclogite at 700 to 1400 degrees C. *Earth Planet. Sci. Lett.* **237**, 873-892.

KLEMM, L., PETTKE, T., GRAESER, S., MULLIS, J. & KOUZMANOV, K. (2004): Fluid mixing as the cause of sulphide precipitation at Albrunpass, Binn Valley, Central Alps. *Schweiz. Mineral. Petrogr. Mitt.* **84**, 189-212.

KLEMM, L. M., PETTKE, T., HEINRICH, C.A. & CAMPOS, E. (2007): Hydrothermal evolution of the El Teniente deposit, Chile: Porphyry Cu–Mo ore deposition from low-salinity magmatic fluids. *Econ. Geol.* 102, 1021-1045.

KLEMM, L.M., PETTKE, T. & HEINRICH, C.A. (2008): Fluid and source magma evolution of the Questa porphyry Mo deposit, New Mexico, USA. *Mineralium Deposita,* in press.

LAMBRECHT, G., DIAMOND, L.W. & PETTKE, T. (2008): Modification of gas speciation in quartz-hosted fluid inclusions by stray laser radiation during LA–ICP–MS analysis. *Am. Mineral.* **93**, 1187-1190.

LANDTWING, M.R., PETTKE, T., HALTER, W.E., HEINRICH, C.A., REDMOND, P.B., EINAUDI, M.T. & KUNZE, K. (2005): Copper deposition during quartz dissolution by cooling magmatic–hydrothermal fluids: The Bingham porphyry. *Earth Planet. Sci. Lett.* **235**, 229-243.

LATKOCZY, C. & GÜNTHER, D. (2002): Enhanced sensitivity in inductively coupled plasma sector field mass spectrometry for direct solid analysis using laser ablation (LA–ICP–SFMS). *J. Analyt. Atom. Spectrom.* **17**, 1264-1270.

LONGERICH, H.P., FRYER, B.J. & STRONG D.F. (1987): Determination of lead isotope ratios by inductively coupled plasma–mass spectrometry (ICP–MS). *Spectrochim. Acta Part B-Atom. Spectrosc.* **42**, 39-48.

LONGERICH, H.P., GÜNTHER, D. & JACKSON, S.E. (1996a): Elemental fractionation in laser ablation inductively coupled plasma mass spectrometry. *Fres. J. Analyt. Chem.* **355**, 538-542.

LONGERICH, H.P., JACKSON, S.E. & GÜNTHER, D. (1996b): Laser ablation inductively coupled plasma mass spectrometric transient signal data acquisition and analyte concentration calculation. *J. Analyt. Atom. Spectrom.* **11**, 899-904.

LOUCKS, R.R. & MAVROGENES, J.A. (1999): Gold solubility in supercritical hydrothermal brines measured in synthetic fluid inclusions. *Science* **284**, 2159-2163.

LÜDERS, V., REUTEL, C., HOTH, P., BANKS, D.A., MINGRAM, B. & PETTKE, T. (2005): Fluid and gas migration in the North German Basin: fluid inclusion and stable isotope constraints. *Intl. J. Earth Sci.* **94**, 990-1009.

MANK A.J.G. & MASON P.R.D. (1999): A critical assessment of laser ablation ICP–MS as an analytical tool for depth analysis in silica-based glass samples. *J. Analyt. Atom. Spectrom.* **14**, 1143-1153.

MASON, P. (2001): Expanding the capabilities of laser-ablation ICP–MS with collision and reaction cells. *In* Laser Ablation in the Earth Sciences (P. Sylvester, ed.). *Mineral. Assoc. Can. Short Course Series Volume* **29**, 63-82.

MASON, P.R.D., NIKOGOSIAN, I.K. & VAN BERGEN, M. (2008): Major and trace element analysis of melt inclusions by laser ablation ICP–MS. *In* Laser Ablation ICP–MS in the Earth Sciences: Current Practices and Outstanding Issues (P. Sylvester, *ed.*). *Mineral. Assoc. Can. Short Course Series* **40**, 219-239.

MCKIBBEN, M.A. (2007): Effect of host mineral species on post-trapping changes in fluid inclusion composition – an equilibrium modeling approach. GSA Annual Meeting, 28-31 October 2007, Denver, USA.

MOENS, L., VANHAECKE, F., RIONDATO, J. & DAMS, R. (1995): Some figures of merit of a new double focusing inductively-coupled plasma–mass spectrometer. *J. Anal. At. Spectrom.* **10**, 569-574.

NAMBU M. & SATO T. (1981) The analysis of fluid inclusions in The microgram range with an ion microanalyzer. *Bull. Minéral.* **104**, 827-833.

PETTKE, T. (2006): *In situ* laser-ablation ICPMS analysis of melt inclusions and prospects for constraining subduction zone magmatism. *In* Melt Inclusions in Plutonic Rocks (J. D. Webster, ed.). *Mineral. Assoc. Can. Short Course Series Volume* **36**, 51-80.

PETTKE, T. & DIAMOND, L.W. (1995): Rb–Sr isotopic analysis of fluid inclusions in quartz: Evaluation of bulk extraction procedures and geochronometer systematics using synthetic fluid inclusions. *Geochim. Cosmochim. Acta* **59**, 4009-4027.

PETTKE, T. & KLEMM, L.M. (in prep.): A novel analyte jumping routine for the representative recording of fast transient signals in LA–ICP–MS. *J. Analyt. Atom. Spectrom.*, to be submitted.

PETTKE, T., DIAMOND, L.W. & KRAMERS, J.D. (2000a): Mesothermal gold lodes in the north-western Alps: A review of genetic constraints from radiogenic isotopes. *Eur. J. Mineral.* **12**, 213-230.

PETTKE, T., HEINRICH, C.A., CIOCAN, A.C. & GÜNTHER, D. (2000b): Quadrupole mass spectrometry and optical emission spectroscopy: detection capabilities and representative sampling of short transient signals from laser-ablation. *J.*

Analyt. Atom. Spectrom. **15**, 1149-1155.

PETTKE, T., WIECHERT, U.H., AUDÉTAT, A., GÜNTHER, D. & HEINRICH, C.A. (2003): Can accurate Pb isotopic compositions be determined on single fluid inclusions? *Geochim. Cosmochim. Acta* **67**, A378-A378.

PETTKE, T., HALTER, W.E., WEBSTER, J.D., AIGNER-TORRES, M. & HEINRICH, C.A. (2004): Accurate quantification of melt inclusion chemistry by LA–ICPMS: a comparison with EMP and SIMS and advantages and possible limitations of these methods. *Lithos* **78**, 333-361.

PETTKE, T., OBERLI, F., AUDÉTAT, A., WIECHERT, U.H., HARRIS, C.R. & HEINRICH, C.A. (2008): Precise and accurate lead isotopic analysis of fast transient signals by laser-ablation MC–ICP–MS. Abstract. 18th Annual Goldschmidt Conference, July 13-18, Vancouver, Canada.

PETTKE, T., OBERLI, F., AUDÉTAT, A., WIECHERT, U.H., HARRIS, C.R. & HEINRICH, C.A. (in prep.): Precise and accurate lead isotopic analysis of fast transient signals by laser-ablation MC–ICP–MS. *J. Analyt. Atom. Spectrom.*, to be submitted.

RAMSEY, M.H., COLES, B.J., WILKINSON, J.J. & RANKIN, A.H. (1992): Single fluid inclusion analysis by laser ablation inductively coupled llasma atomic emission spectrometry – quantification and validation. *J. Analyt. Atom. Spectrom.* **7**, 587-593.

ROEDDER, E. (1984): Fluid Inclusions. *In* Reviews in Mineralogy (P. H. Ribbe, ed.) *Mineral. Soc. Am.,* **12**, 646p.

RUSK, B.G., REED, M.H., DILLES, J.H., KLEMM, L.M. & HEINRICH, C.A. (2004): Compositions of magmatic hydrothermal fluids determined by LA–ICP–MS of fluid inclusions from the porphyry copper–molybdenum deposit at Butte, MT. *Chem. Geol.* **210**, 173-199.

SCAMBELLURI, M., MUNTENER, O., OTTOLINI, L., PETTKE, T.T. & VANNUCCI, R. (2004): The fate of B, Cl and Li in the subducted oceanic mantle and in the antigorite breakdown fluids. *Earth Planet. Sci. Lett.* **222**, 217-234.

SHEPHERD, T.J. & CHENERY, S.R. (1995): Laser-ablation ICP–MS elemental analysis of individual fluid inclusions – an evaluation study. *Geochim. Cosmochim. Acta* **59**, 3997-4007.

SHIBUYA, E.K., SARKIS, J.E.S., ENZWEILER, J., JORGE, A.P.S. & FIGUEIREDO, A.M.G. (1998): Determination of platinum group elements and gold in geological materials using an ultraviolet laser ablation high-resolution inductively coupled plasma mass spectrometric technique. *J. Analyt. Atom. Spectrom.* **13**(9), 941-944.

SIMON, A.C., PETTKE, T., CANDELA, P.A., PICCOLI, P.M. & HEINRICH, C.A. (2004): Magnetite solubility and iron transport in magmatic–hydrothermal environments. *Geochim. Cosmochim. Acta* **68**, 4905-4914.

SIMON, A.C., FRANK, M.R., PETTKE, T., CANDELA, P.A., PICCOLI, P.M. & HEINRICH, C.A. (2005): Gold partitioning in melt–vapor–brine systems. *Geochim. Cosmochim. Acta* **69**, 3321-3335.

SPANDLER, C., MAVROGENES, J. & HERMANN, J. (2007): Experimental constraints on element mobility from subducted sediments using high-P synthetic fluid/melt inclusions. *Chem. Geol.* **239**, 228-249.

SPANDLER, C., PETTKE, T., BERGER, A. & MAGEE, C. (2008): New constraints on the high-field-strength element concentration of NIST SRM 610 and 612 glasses. Abstract. 18th Annual Goldschmidt Conference, July 13-18, Vancouver, Canada.

SPANDLER, C., PETTKE, T., BERGER, A., ULMER, P. & MAGEE, C. (in preparation): Reference element concentrations of NIST SRM 610 and 612 glasses: Consistency evaluation and new constraints on high field strength element data.

STERNER, S.M. & BODNAR, R.J. (1989): Synthetic fluid inclusions.7. Re-equilibration of fluid inclusions in quartz during laboratory-simulated metamorphic burial and uplift. *J. Metam. Geol.* **7**, 243-260.

STOFFELL, B., WILKINSON, J.J. & JEFFRIES, T.E. (2004): Metal transport and deposition in hydrothermal veins revealed by 213nm UV laser ablation microanalysis of single fluid inclusions. *Am. J. Sci.* **304**, 533-557.

SYLVESTER, P.J. (2008): Matrix effects in laser ablation–ICP–MS. *In* Laser Ablation ICP–MS in the Earth Sciences: Current Practices and Outstanding Issues (P. Sylvester, *ed.*). *Mineral. Assoc. Can. Short Course Series* **40**, 67-78.

TANNER, S.D. & BARANOV, V.I. (1999): Theory, design, and operation of a dynamic reaction cell for ICP–MS. *Atom. Spectrosc.* **20**, 45-52.

TSUI, T.F. & HOLLAND, H.D. (1979): Analysis of fluid inclusions by laser microprobe. *Econ. Geol.* **74**, 1647-1653.

ULRICH, T., GÜNTHER, D. & HEINRICH, C.A. (2002): Evolution of a porphyry Cu–Au deposit, based on LA–ICP–MS analysis of fluid inclusions: Bajo de la Alumbrera, Argentina. *Econ. Geol.* **97**, 1888-1920.

VENABLE, J. & HOLCOMBE, J.A. (2001): Peak broadening from an electrothermal vaporization sample introduction source into an inductively coupled plasma. *Spectrochim. Acta Part B-Atom. Spectrosc.* **56**, 1431-1440.

WILKINSON, J.J., RANKIN, A.H., MULSHAW, S.C., NOLAN, J. & RAMSEY, M.H. (1994): Laser ablation–ICP–AES for the determination of metals in fluid inclusions – an application to the study of magmatic ore fluids. *Geochim. Cosmochim. Acta* **58**, 1133-1146.

WOODHEAD, J. (2002): A simple method for obtaining highly accurate Pb isotope data by MC–ICP–MS. *J. Analyt. Atom. Spectrom.* **17**, 1381-1385.

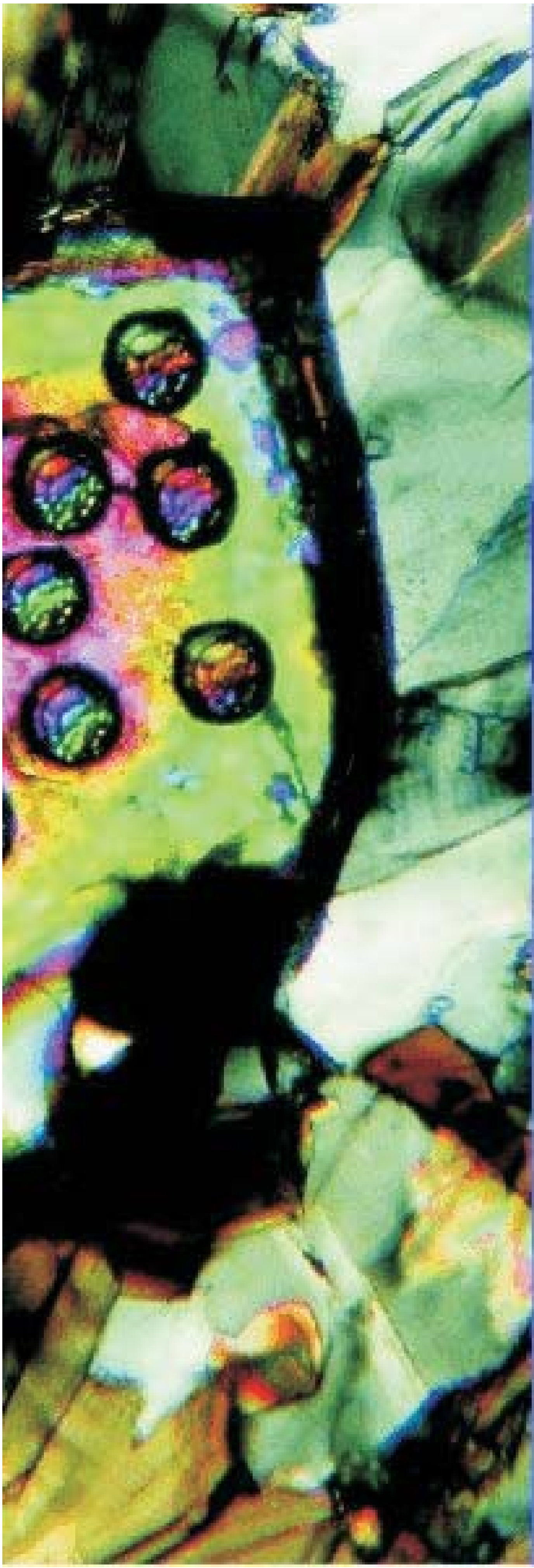

Mineralogical Association of Canada

Laser Ablation ICP-MS in the Earth Sciences: Current Practices and Outstanding Issues

Editor
Paul Sylvester

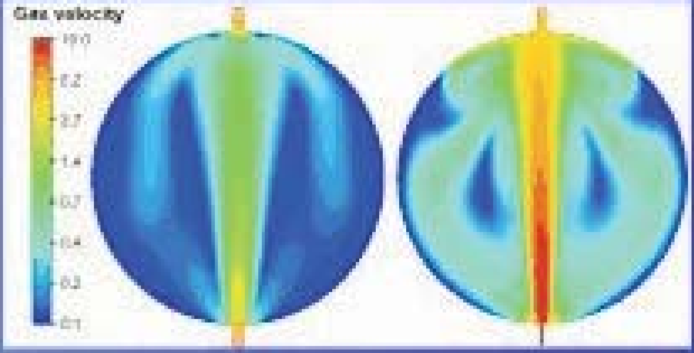

Short Course Series
Volume
40

VANCOUVER, BC, 2008
Series Editor
Robert Raeside